U. of Iowa 68-17
Revised May 1968

N 69-23135

FACILITY FORM 602

(ACCESSION NUMBER)	(THRU)
61	1
(PAGES)	(CODE)
CR# 100604	30
(NASA CR OR TMX OR AD NUMBER)	(CATEGORY)

Department of Physics and Astronomy

THE UNIVERSITY OF IOWA

Iowa City, Iowa

U. of Iowa 68-17
(Revised May 1968)

Effect of $2 < \lambda < 12$ A° Solar X-Rays on the Ionosphere Between 60 and 100 km*

by

P. R. Sengupta

Department of Physics and Astronomy
The University of Iowa
Iowa City, Iowa

March 1968

*This work was supported in part by the National Aeronautics and Space Administration under Contract No. NAS5-9076.

ABSTRACT

Computations have been made in order to evaluate the ionospheric effects caused by the observed $2 < \lambda < 12$ A° x-ray quiescent flux and flare flux. Of seventy-two solar x-ray flares having F(2-12 A°) greater than 3×10^{-3} erg/cm^2 sec as recorded by the University of Iowa detector on Explorer 33 sixty-seven are found to be accompanied by reported S.I.D.'s in which the electron density of the ionosphere between 60 to 100 km undergoes a rapid increase during a few minutes. These rapid increases in electron density are presumably caused by the enhanced x-ray flux in the wavelength range $1 < \lambda < 10$ A° because softer x-rays would be completely absorbed above 100 km and harder x-rays would penetrate below 60 km without significant attenuation at higher altitudes. The altitudes for peak electron production range from 99 km for 10 A° x-rays down to 58 km for 1 A° x-rays. The electron-production rate equations have been solved using a quiescent x-ray energy spectrum and a mean flare x-ray energy spectrum derived from the work of various observers during the past nine years. The physical and chemical processes involved in the mechanism of ionization of the local atmospheric constituents according to existing models are discussed.

Distribution of the computed electron production rate and the resulting electron density with height have been plotted for quiescent and flare conditions. These plots have been compared with earlier work and available experimental data. It is confirmed that the S.I.D.'s can be explained quantitatively assuming flare x-rays as the only ionizing agent. It is further shown that under 1966 quiescent conditions x-ray ionization in the region under study is comparable to ionization by solar Lyman alpha. Solar Lyman α flux is known to be very steady varying by a factor not more than 2 between solar minima and solar maxima; while 0 - 10 A° solar x-ray flux varies greatly with solar activity (see text). Solar x-rays of wavelength below 10 A° are thus responsible for both rapid variations and day to day variations of the D region electron density. The variation of the effective height of the D region with solar activity may also be traced to the variation of 0 - 10 A° solar x-ray flux.

I. INTRODUCTION

It is now known that E layer of the Ionosphere is mainly due to 10 - 20 A° and 31 - 100 A° solar x-rays. X-rays of wavelength less than 10 A° penetrate below 100 km without appreciable loss of energy at higher levels. It is, therefore, expected that 0 - 10 A° x-rays would contribute to D region ionization. 2 - 12 A° x-ray flux data is now available from University of Iowa detectors on Explorer 33 and Explorer 35 satellites. 2 - 8 A° x-ray data is available from Mariner V satellite. It is possible to obtain the flux below 10 A° from the available data assuming quiescent sun x-ray emission to be thermal in nature with $Te = 2 \times 10^{6}$°K [Sengupta, P. R., 1968]. X-ray flux below 10 A° varies within wide limits over a period and was found to lie between $\sim 5 \times 10^{-4}$ to $\sim 6 \times 10^{-3}$ erg/cm^2 sec during the period July to November 1966. Ionization at the D region height due to the quiescent sun flux recorded during the period is comparable with the total ionization in this region on a day of high solar activity.

The effect of 0 - 10 A° x-rays is more pronounced during a solar flare. Solar flares are known to cause a variety of simultaneous ionospheric effects, occurring principally in the D region.

These effects, called Sudden Ionospheric Disturbances (S.I.D.s), include, amongst others, the following:

(1) Shortwave fade out (S.W.F.) observed as an abrupt decrease in the field strength of high frequency radio signals.

(2) Sudden increase in the signal strength received from distant L. F. and V.L.F. stations (S.E.S.).

(3) Sudden enhancement of atmospheric noise (SEA) on frequencies upto 100 kc/s.

(4) Sudden changes in phase (SPA) of received signal, first measured by Bracewell and Starker [1949] on 16 kc/s, and later extended to other frequencies in the V.L.F. region.

(5) Sudden enhancement of cosmic noise absorption observed generally in the neighborhood of 20 mc/s (S.C.N.A.).

(6) Sudden frequency deviations (S.F.D.), observed on highly stable-frequency transmissions, first reported by Watts and Davies [1960].

It is known that, excepting the S.F.D., the others arise from a sudden increase in the ionization below 100 km. The S.F.D.s originate in the E or F region, the exact level being determined by frequency used and the range of path.

Enhancement of solar radiation in the x-ray and ultra-violet regions have been measured with fairly reliable accuracy in rocket and satellite experiments during the past twelve years. X-ray measurements were generally carried out in a number of bands, e.g., 0 - 8 A°, 2 - 12 A°, 8 - 20 A°, 44 - 60 A°, and 22 - 100 A° as integrated fluxes; but for a few events spectral data are also available. Satellite observations of x-ray flares come principally from the NRL SR-I, SR-3, SR-4, and SR-8 Satellites; Soviet Space Stations and Electronic Satellites; Ariel I Satellite, the OSO-I and OSO-II Satellites, VELA I and II Satellites; Injun I and III, Explorer 33 and 35, and Mariner V Satellites [Sengupta, P. R., 1968].

Large increase in 0 - 20 A° x-ray flux, often by a factor greater than hundred, was observed in all cases of x-ray flare. A hardening of x-ray spectrum also was observed. Relative increase in 44 - 60 A° flux was found to be much less than relative increase in 0 - 20 A° flux.

Observations on changes in EUV radiation during flares came principally from OSO Satellites [Neupert, 1964]. Changes were observed in He II, Fe XV, and Fe XVI emissions. For the flare of 27 April 1962, considered typical, enhancement was about 12% in He II, 10% in Fe XV, and 50% in Fe XVI.

For Lyman-alpha, long believed to be a major source of flare time ionization, both rocket and satellite observations have shown little change. OSO-I observations have shown that out of seven class 2 flares, Lyman-alpha enhancement was greater than 30% for 2, 1 to 3% for one and none for 4 [Neupert, 1964].

There is thus strong evidence that the rapid increase in ionization in the region below 100 km, ie,in the D region observed during a flare is caused by x-rays of wavelength less than 10 A°, because x-rays of longer wavelength lose most of their energy at higher altitudes (see Figure 9).

University of Iowa detector on Explorer 33 detected a large number of x-ray flares during July - August 1966. Several of them were large flares with peak intensity greater than 10^{-2} erg/cm^2 sec. Many small flares with peak intensity less than 10^{-3} erg/cm^2 sec, were also recorded. Seventy-two flares with peak intensity greater than 3×10^{-3} erg/cm^2 sec are chosen for the present study. Sixty-seven of these flares are found to be accompanied by reported S.I.D.s. Table I gives the x-ray flares together with associated S.I.D.s. A detailed statistical analysis of the correlation between the x-ray flares and the associated S.I.D.s will be presented in another paper. In this paper increase in ionization due to two typical flares, one large flare on 7 July 1966 and another medium flare on 31 August 1966, has been computed to show that the observed ionospheric effects associated with these two events are explained by the ionization between 60 to 100 km due to enhanced 0 - 10 A° flux.

II. INSTRUMENTATION

The Explorer 33 satellite was launched on July 1966 into an eccentric orbit about the earth with its initial apogee at a geocentric radial distance of 440,000 km. The satellite is spin stabilized but there are weak torques due, primarily, to solar radiation pressure, which produce slow changes in the spin period and the celestial coordinates of the spin axis of the satellite. In July 1966 the spin period was 2.286 seconds and right accession and declination of the spin axis were 225.1° and - 21.2° respectively [Van Allen, J. A., 1967].

The system of University of Iowa 2 - 12 A° x-ray detectors comprise the following:

GM1: An EON 6213 mica window G. M. tube having a 1.7 mg/cm^2 thickness window and a fan shaped aperture whose central axis is orthogonal to the spin axis of the satellite.

GM2: A similar G. M. tube with 1.3 mg/cm^2 thick mica window and a conical aperture of 20° half angle, whose axis is parallel to the spin axis.

GM3: A similar G. M. tube with 1.3 mg/cm^2 thickness mica window and a conical aperture of 20° half angle, whose axis is anti-parallel to the spin axis.

The arrangement of the detectors is shown in Figure 1. The three counters face the sun one after another in the course of a year with a 19 days dark interval in-between when no counter would see the sun. The aspect angle α of the counters varies continuously and can be calculated knowning the position of the satellite. A correction factor $f(\alpha)$ for relevant values of α has been obtained experimentally for each detector. Figure 2 shows a plot of $f(\alpha)$ for GM1 on different satellite days. Similar plots are available for GM2 and GM3. The counters record both x-rays and charged particles. In order to obtain x-ray flux, particle flux has to be subtracted from the total signal of the detector. This is achieved in the following way: (1) when GM2 is facing the sun, GM3 will be in the shadow, and vice versa. Hence one of them, which is facing the sun will record solar x-ray and particles while the other one will record only particles. Difference of the two signals will then give the x-ray flux. (2) when GM1 is facing the sun, use is made of a spin sector generator (see Figure 3). A spin sector generator triggered by a see-sun pulse, gates pulses from GM1 into four quadrants, the accumulated output of each over a 25.57 second period being transmitted separately. The spin axis lies within 4° of the ecliptic plane. Hence the four quadrants of the GM1 detector respond as follows:

Sector I - particles only

Sector II - particles only

Sector III - solar x-rays and particles

Sector IV - particles only

Hence the x-ray flux GIX is obtained by the relation

$$GIX = R_{III} - (R_I + R_{II} + R_{III})/3$$

where R_i is the counting rate of the ith sector [Van Allen, J. A., 1967].

The x-ray efficiency of the detectors have been determined by two methods: (1) by calculation, (2) by experimental comparison with a longer pathlength Be window, argon filled EON 6312 tube whose efficiency can be calculated with better accuracy. The efficiency curves are given in Figures 4 and 5. It is seen from Figure 5 that

$$2 - 12 \text{ A}^\circ \text{ flux} = \text{no. of counts} \times 1.8 \times 10^{-6} \text{ erg/cm}^2 \text{ sec}$$

is a good approximation for any observed form of solar x-ray spectrum, including one having a distribution of emission lines superimposed on a continuum. This value is adopted for calculations of absolute energy flux [Van Allen, J. A., 1967]. The detectors have a high sensitivity and large dynamic range. Time resolution of the telemetered signal is 81 seconds and the telemetry is independent of spin period. The system of detectors has been recording 2 - 12 A° x-ray flux since 1 July 1966 and has recorded several hundred x-ray flares - some with fairly high peak flux. But the signal is never seen to saturate.

Ionospheric data used in this paper are taken from Solar Geophysical data bulletin published monthly by ESSA, Boulder, under the auspices of U. S. Department of Commerce.

22 mc/s S.C.N.A. over Penticton for 7 July 1966 event (Figure 17) is taken from a published paper by J. A. Van Allen [1967].

III. THEORY AND COMPUTATIONS

The principal ionization processes in the D region are:

(1) Nitric oxide ionized by Lyman-alpha.

(2) Molecular oxygen and Nitrogen ionized by x-rays of wavelength less than 10 A°.

(3) Molecular oxygen and Nitrogen ionized by cosmic rays.

In the present work, we are concerned only with the ionization by 0 - 10 A° x-rays.

As the x-rays are absorbed on their way through the atmosphere, their intensity will decrease with decreasing altitude. The fraction of x-ray intensity $d\varphi/\varphi$ absorbed in the height interval between h and h + dh is given by

$$d\varphi/\varphi = -\Sigma\ \sigma i\ Ni(h)\ \sec\chi\ dh \qquad (1)$$

where χ is the angle between the zenith and the direction of the x-ray beam, σi is the absorption cross-section per atom of the ith species of the atmospheric constituents, and Ni(h) is the number density of the species. In Figures 6 and 7 values of σ used in the present work for oxygen and Nitrogen for different values of λ are given. For Ni(h) CIRA [1965] mean atmospheric model has been used.

$\sum_i \sigma i\ Ni(h)$ can be replaced by the average mass absorption coefficient of the atmosphere times the atmospheric density; i.e.

$$\sigma\,\rho(h) = \Sigma\ \sigma i\ Ni(h) \qquad (2)$$

Integrating both sides of equation (1) and solving for φ we have

$$\varphi(h) = \varphi_o[\exp(-\sigma\, N(h)\ \sec\chi)]$$

$$= \varphi_o \exp[-\tau(h)] \qquad (3)$$

where

$$N(h) = \int_h^\infty \rho(h)\ dh$$

and $\tau(h)$, called the optical depth of the photon at the height h is given by

$$\tau(h) = \sigma\, N(h)\ \sec\chi \qquad (4)$$

values of N(h) between 50 and 100 km are computed from CIRA [1965] mean atmospheric model. These values are given in Table II. σ is the average effective cross-section and φ_o the flux density outside the atmosphere.

The assumption made above is that once a photon is scattered, it is destroyed i.e. a photon loses all its energy in the same region. This is reasonable because a photon will most probably lose energy upon scattering, so the probability that the photon will travel much further downward is considerably smaller because of the greatly increased absorption coefficient for the lower energy photons.

The rate of production of the ith species of the positive ion is the rate at which photons are scattered from that species times the yield per photon.

The rate of electron production is the total rate of positive ion production and is given by

$$q(h) = W \sum_i \sigma i \; Ni(h) \; ri \; \varphi(h)$$

$$= \eta \; \sigma \; \rho(h) \; \varphi(h) \qquad (5)$$

where W is the photon energy in electron volt. ri is the electron yield per electron volt for the ith species, η is the average ionization efficiency of the photon. The assumption has been made that the incident photon yields all its energy at one altitude, and that the electrons will not migrate to different altitudes very rapidly. Equation (5) can also be written as

$$q(h) = \varphi_o \cos \chi \, \eta \frac{\tau}{Ho} \exp(-\tau)$$

where

$$\rho(h) = \rho(ho) \exp(-\frac{h-ho}{Ho}) \qquad (6)$$

ho = arbitrary reference height

Ho = the scale height (assumed to be constant within the heights of interest)

and

$$\tau = \sigma N(h) \sec \chi \simeq \sigma \rho_o Ho \sec \chi, \text{ the optical depth.} \qquad (7)$$

The peak photoionization occurs at the height where $\tau = 1$, and is given by:

$$q \text{ peak} = \frac{\eta \varphi_o}{Hoe} \qquad (8)$$

If the reference height (ho) is taken as the height at which the maximum ionization occurs, i.e., the height at which $\tau = 1$ when $\chi = 0$, then the height of the peak production for any value of χ is given by

$$h\ peak = ho + Ho\ \ln(\sec \chi) \qquad (9)$$

Equations (5), (6), (7), (8), and (9) indicate:

(1) The photoionization is linearly proportional to the x-ray flux.

(2) At heights ($h - ho \gg Ho$), where the optical depth is small and flux is large, the ionization rate is proportional to the solar flux above the atmosphere, the particle density, the absorption cross-section, and the ionization efficiency of the photon.

(3) The peak ionization is proportional to cos χ.

(4) The height of peak production increases with increasing solar zenith angle.

(5) Below the height of peak production where $\tau > 1$, the ionizing flux and photoionization rapidly decreases with decreasing height.

Heights of maximum ionization for different values of λ are computed and plotted in Figure 8.

The total number of electrons per square centimeter in a vertical column is given by

$$Q = \int_0^\infty q(h)\, dh \qquad (10)$$

This integral is easily evaluated if it is remembered that $dN(h)/dh = \rho(h)$. The result is simply

$$\int_0^\infty q\, dh = \varphi_o \int_0^\infty \sigma\rho\, Wr[\exp(-\sigma N(h) \sec \chi]\, dh$$

$$= \varphi_o\, Wr \cos \chi$$

$$= \varphi_o\, \eta \cos \chi \qquad (11)$$

Therefore the total number of electrons produced in a vertical column is proportional to the energy flux from the sun, the cosine of the zenith angle and the ionization efficiency of the photon.

For a continuous spectrum of incident photons the photo-ionization rate may be calculated from the equation

$$q(h) = \int_0^{\lambda} q(\lambda)\, d\lambda$$

$$= \int_0^{\lambda} \eta(\lambda)\sigma(\lambda)\rho(h)\varphi(\lambda, h)\, d\lambda$$

$$= \int \eta(\lambda)\sigma(\lambda)\rho(h)\ \varphi_0(\lambda)\ \exp[-\ \tau(\lambda, h)\ d\lambda \qquad (12)$$

Ion production rates per unit flux incident normally ($\chi = 0$) at the top of the atmosphere computed with equation (5) for $\lambda = 2$ A°, 5 A° and 8 A° are given in Figure 9.

Ionization rates due to quiescent sun 0 - 10 A° flux are computed with equation (12) for two values of the flux: 6×10^{-3} erg/cm^2 sec and 0.5×10^{-3} erg/cm^2 sec. These values are representative of high and low solar activity levels respectively. The x-ray spectrum used is given in Figure 10. Ionization rate due to Lyman α flux is computed for a flux of 4.8 erg/cm^2 sec. This is representative of the flux recorded by OSO satellites (Neupert, 1964). Computations are made for $\chi = 0$. The computed values of q are given in Figure 11 along with values of q due to galactic cosmic radiation computed by Webber for mid-latitudes. The observed values of q are obtained from the electron density profile reported from rocket experiments in 1962 over Wallops Island in October 1962

[Smith, 1963] and from partial reflection measurements in 1964 [Deeks, 1964].

For computing Δq due to flare x-ray, it is necessary to know the spectral energy distribution. Figure 12 gives probable spectral energy distributions for different types of flare. The three spectral distributions are obtained as the mean of the spectral measurements made in rocket and satellite experiments during past 9 years [Sengupta, P. R., 1968]. Distribution A would correspond to impulsive hard x-ray flares. Distribution B may be taken as representative of strong soft x-ray flares and agrees well with the spectral distributions of the x-ray flare on 27 April 1962, measured by Ariel I Satellite. Distribution C would correspond to weak flares. Enhanced production rates computed for flares on 7 July 1966 and 31 August 1966 for $\chi = 0$, are given in Figure 13. Spectral distribution B in Figure 12 is used for the computation.

For the D region the electron continuity equation assumes the form:

$$\frac{dn}{dt} = q/(1 + \lambda_n) - \alpha' n^2 \qquad (13)$$

where α', the effective recombination coefficient, consists of two parts: one α_c, essentially constant, and determined by dissociative recombination coefficient of the principal molecular ion; and the other controlled by the negative ion-to-electron ratio λ_n, varying rapidly with height. The expression for α' is:

$$\alpha' = \alpha_c + \lambda_n \alpha_i \qquad (14)$$

where α_i is the ion recombination coefficient.

Under equilibrium conditions, therefore, the expression for the excess electron density Δn is:

$$\frac{\Delta q}{1 + \lambda_n} = \alpha' \Delta n^2 + 2\alpha' n \Delta n \qquad (15)$$

where Δq is the excess ion production rate due to the x-ray flare and is given by Equation (12).

If

$$n \Delta n << \Delta n^2$$

then

$$\Delta q/(1 + \lambda_n) \approx \alpha' \Delta n^2 \qquad (16)$$

Equation (16) is used for computing excess electron density due to the two x-ray flares. Values of α' and λ_n used are given in Figure 14 [Mitra, 1964; Belrose, 1964]. The computed electron densities are plotted in Figure 15.

Let k be the absorption per unit path suffered by the incident cosmic radio noise of angular frequency ω in passing through the ionosphere, and A the total absorption suffered, then

$$A = \int_0^\infty k \, dh \tag{17}$$

It is convenient to introduce another parameter, $k_o = k/n$, where k_o now expresses the absorption per unit path per unit electron. Instead of computing k_o from the usual Appleton-Hartree magnetoionic equations, use has been made of the tables published by Chorbajian, Suguira and Parthasarathy [1962] for absorption computed with Sen-Wyller generalization of the magnetoionic formula which take into account the dependence of the collision frequency on the electron velocity. The calculations, however, were made for the magnetic field of College, Alaska (0.57 gauss), and they will differ for places where the field is sensibly different. Above 20 mc/s, however, the magnetic field control of the absorption values is trivial.

Writing Ax as the additional absorption during a solar flare, we have:

$$Ax = \int_0^h [\Delta q/(1 + \lambda_n)(\alpha_c + \lambda_n \alpha_i)]^{\frac{1}{2}} k_o \, dh \qquad (18)$$

where Δq is given by Equation (12).

Considerable simplification occurs if absorption is contributed principally by levels for which λ_n is negligible. In this case,

$$Ax = \int_0^h (\Delta q/\alpha')^{\frac{1}{2}} k_o \, dh \qquad (19)$$

Another simplification occurs when $\alpha_c = \alpha_i$. This is not an entirely unreasonable assumption, since recent laboratory observations indicate

$\alpha_D(N_2) = (2.8 \pm 0.5) \times 10^{-7}$ cm^3/sec [Biondi, 1964]

$\alpha_D(O_2) = (2.0 \pm 0.5) \times 10^{-7}$ cm^3/sec [Biondi, 1964]

$\alpha_D(NO) = 3.2 \times 10^{-7}$ cm^3/sec [Doering and Mahan, 1964]

$\alpha_i = 10^{-7}$ cm^3/sec [Greaves, 1959]

This assumption simplifies Equation (18) to:

$$Ax = \int_{o}^{h} \frac{k_o}{1+\lambda_n} (\Delta q/\alpha_c)^{\frac{1}{2}} dh \qquad (20)$$

Equation (20) has been used for computing 22 mc/s. S.C.N.A. between 60 and 100 km for the two x-ray flares. The results are given in Figure 16.

IV. RESULTS AND CONCLUSIONS

Ionization Under Quiet (Non-Flare) Conditions:

0 - 10 A° x-rays are an important source of ionization in the D region. From Figure 11 it is evident that above a certain level (~ 70 km under average conditions) ionization is determined chiefly by 0 - 10 A° flux. Below 70 km x-ray ionization is comparable with ionization due to other sources. In addition to 0 - 10 A° flux, strong C VI line at 33.7 A° contributes considerably between 85 and 100 km. Even at low solar activity level x-ray ionization is comparable with ionization due to Lyman α. Lymna α flux is known to be very constant varying by a factor not more than 2 between solar minima and solar maxima [Friedman, 1961; Whitten and Poppof, 1965]. Thus the background (non-flare) 0 - 10 A° solar x-ray flux, which varies greatly with solar activity, is an important source of free electrons in the D region in two respects. First, the ionization caused by background solar x-rays over-rides other sources of electrons during high solar activity or near solar maxima. Second, even near solar minima daily or hourly variations in electrons concentrations are caused by the fluctuations in 0 - 10 A° flux. It is these fluctuations that make it difficult to correlate measured electron profiles in this region with theory. The variation of D layer height with solar activity

cycle is also explained on the basis of relative importance of x-ray ionization over ionization due to galactic cosmic radiation and Lyman alpha. It should be noted that in view of Equation (13), a difference in the q value of one order of magnitude results in a difference of n values by a factor of 3 only, whereas an error in α' contributes linearly to error in n value. Due to uncertainties about α' in the D region, it is important to compare the ionization rates due to various ionization sources when both q and n are small.

Flare Ionization:

Flare enhancement of the D region electron density is essentially due to 0 - 10 A° x-rays. Following conclusions regarding flare enhancements can be drawn from Figure 15:

(1) Due to x-ray flare on 7 July D layer height was lowered from 72 km to 50 km i.e. by more than 22 km. 31 August event lowered the D layer height by 12 km. S.P.A.s are caused by the lowering of the D layer height. Reported importances of the S.P.A.s associated with the two events are 99 and 42 respectively (see Table I). Thus the S.P.A. importances are well correlated with the computed lowering of heights for the two events.

(2) Relative increase in electron density is more at lower altitudes then at higher altitudes. For 7 July event,

electron density increased by a factor greater than 100 below 60 km, by a factor $\approx$ 50 between 60 and 100 km, by a factor $\approx$ 10 between 70 and 95 km and by a factor $\approx$ 2 above 95 km. Large increase in electron density between 60 and 80 km accounts for most of the S.I.D.s, viz., S.E.A., S.E.S., S.W.F. and a large part of S.C.N.A.

(3) Steepness of the flare electron profile depends on the flare x-ray spectrum used. If the spectrum is steep and has a maximum at about 6 A°, the lower edge of the electron profile will be steep. A flat spectrum will cause flat electron profile. S.P.A., S.E.A. and S.E.S., which depend on the steepness of the electron profile, would be susceptible to the flare x-ray spectrum.

The values of n given in Figure 15 are uncertain by a factor 2 or 3 due to uncertainity in the values of α' used. It is possible to compute α' from S.C.N.A. and other S.I.D. data knowing the flare x-ray flux and spectrum.

Maximum cosmic noise absorption reported for 7 July event is 7 db for 18 mc/s over Maui (χ = 30°). Computed 22 mc/s absorption between 60 and 100 km due to 0 - 10 A° x-ray flare is 5 db for χ = 0. Assuming that absorption varies as cos $\chi^{3/2}$ and remembering that absorption is nearly inversely proportional to square of angular frequency of the cosmic noise, more than 80% of the total absorption took place between 60 and 100 km.

For the event on 31 August the computed 22 mc/s peak absorption between 60 and 100 km is 2.8 db for $\chi = 0$. Reported peak absorption for the event over Manila ($\chi = 50°$) is 1.8 db. From this 22 mc/s absorption for $\chi = 0$ would be 2.5 db. This value is somewhat low because of the fact that for $\chi > 30°$ the height of peak ionization is considerably higher which results in lower total absorption. Allowing a correction for this total 22 mc/s absorption for $\chi = 0$ would be ≈ 3.0 db. Thus in this case, more than 90% of the absorption took place between 60 and 100 km.

These results are significant in view of the fact that the computed values in both the cases have been obtained by considering enhanced ionization due to 0 - 10 A° x-rays only.

Broken line in Figure 17 shows the time-history of the computed and normalized 22 mc/s S.C.N.A. due to 0 - 10 A° x-ray flare on 7 July, and the full line shows the observed 22 mc/s S.C.N.A., over Pentiction. There is complete agreement between the computed and the observed profile.

S.I.D.s are thus primarily due to enhanced ionization between 60 and 100 km caused by 0 - 10 A° x-ray flare.

X-rays of wavelength below 10 A° are responsible for both rapid variations and day to day variations in the D region electron density.

The variation of the effective height of the D region with solar activity may also be traced to the variation of 0 - 10 A° solar x-ray flux.

ACKNOWLEDGMENT

The author is grateful to Professor J. A. Van Allen for providing the necessary facilities for work, for the Explorer 33 x-ray data, and for many useful suggestions.

TABLE I

2-12 A° X-Ray Flares in July-August 1966 with Associated S.I.D.s

No.	Date	Universal Time			Peak 2 - 12 A° Flux	SWF Type	Importance					
		Start	End	Max.	$erg \times 10^{-3}/cm^2 sec$	IMP	ABS	SCNA	SEA	SPA	SES	SFD
1	5-7-66	1841	1858	1851	54							
	5-7-66	1843	1902			SL 1						
	5-7-66	1845	1955							21		
2	5-7-66	2011		2022	72							
	5-7-66	2012	2040	2018							1-	
	5-7-66	2015	2040	2025			12	1				
	5-7-66	2016	2036	2026		SL 1						
	5-7-66	2019	2025	2022								05
	5-7-66	2020	2150							54		
3	5-7-66	2227		2231	82							
	5-7-66	2230	2248	2234						21		
4	6-7-66	0037	0117	0043	32							
	6-7-66	0039	0119	0049						12		
5	6-7-66	0328		0345	28							
	6-7-66	0328	0359	0346		G 1						
	6-7-66	0333	0401	0351						11		
	6-7-66	0336	0335	0347			16	1-				
	6-7-66	0337	0357	0351					1-			
6	6-7-66	0421	0436	0427	38							
	6-7-66	0421	0432	0425		Sl -						
	6-7-66	0421	0444	0426			12	1-				
	6-7-66	0421	0450	0426						22		
	6-7-66	0421	0455	0423							1	

TABLE I CONT.

2-12 A° X-Ray Flares in July-August 1966 with Associated S.I.D.s

No.	Date	Universal Time			Peak 2-12 A° Flux $erg X10^{-3}/cm^2 sec$	SWF Type IMP	Importance					
		Start	End	Max.			ABS	SCNA	SEA	SPA	SES	SFD
7	6-7-66	0530	0547	0537	57							
	6-7-66	0532	0538	0534								16
	6-7-66	0533	0550	0535		S 1						
	6-7-66	0533	0609	0538						51		
	6-7-66	0533	0611	0537			20	1				
	6-7-66	0534	0615	0542							1	
8	6-7-66	1758			> 22							
	6-7-66	1758	1807	1802								15
9	6-7-66	2029		2035	34							
	6-7-66	2030	2037	2032								06
	6-7-66	2035	2105							32		
10	6-7-66	2116		2122	29							
	6-7-66	2117	2120	2118								09
	6-7-66	2117	2148	2121						15		
11	6-7-66	2148	2204	2153	48							
	6-7-66	2149	2153	2151								10
	6-7-66	2149	2201	2152			18	1				
	6-7-66	2150	2206	2152							1	
	6-7-66	2150	2220	2156						64		
12	6-7-66	2223	2252	2229	50							
	6-7-66	2224	2314	2231						33		
	6-7-66	2225	2240	2233		G 1						
	6-7-66	2225	2246	2227							1-	
	6-7-66	2230	0030							43		

TABLE I CONT.

2-12 A° X-Ray Flares in July-August 1966 with Associated S.I.D.s

No.	Date	Universal Time			Peak 2-12 A° Flux $erg \times 10^{-3}/cm^2 sec$	SWF Type IMP	Importance					
		Start	End	Max.			ABS	SCNA	SEA	SPA	SES	SFD
13	7-7-66	0023	0318	0042	280							
	7-7-66	0023	0129	0230D							3+	
	7-7-66	0025		0055						99		
	7-7-66	0025	0329	0026		S 3						30
	7-7-66	0026	0042	0027								
	7-7-66	0026	0142	0033				2				
	7-7-66	0026	0210	0040			56	3				
	7-7-66	0027	0117				80	3				
14	8-7-66		1224	1218	30					99		
	8-7-66	1210		1216							1	
	8-7-66	1214	1230	1219								
	8-7-66	1215	1230	1221			32	2				
	8-7-66	1215	1238	1218					1+			
	8-7-66	1220	1335	1248		S 2						
15	8-7-66	1233	1330	1245	35						1	
	8-7-66	1235	1305U	1250								
	8-7-66	1237	1319	1248			34	2				
	8-7-66	1238	1350	1244					2			
	8-7-66	1238	1415	1250						30		
16	8-7-66	1705	1750	1721	28							14
	8-7-66	1708	1714	1711							2	
	8-7-66	1708	1745	1717								
	8-7-66	1708	1800	1720				3				
	8-7-66	1710	1740D					1-				
	8-7-66	1710	1744	1718		SL 1+						
	8-7-66	1723	1724									

TABLE I CONT.

2-12 A° X-Ray Flares in July-August 1966 with Associated S.I.D.s

No.	Date	Universal Time Start	Universal Time End	Universal Time Max.	Peak 2-12 A° Flux erg x $10^{-3}/cm^2 sec$	SWF Type IMP	Importance ABS	Importance SCNA	Importance SEA	Importance SPA	Importance SES	Importance SFD
	8-7-66	1725	1728	1726								03
	8-7-66	1751	1756	1754								04
17	8-7-66	2122		2130	15							
	8-7-66	2123	2210	2135						58		
	8-7-66	2128	2142	2131							1+	
	8-7-66	2128	2145	2140		G 1						
	8-7-66	2140	2142									
	8-7-66	2140	2210	2145			**	5				
	8-7-66	2142	2148									
	8-7-66	2143	2153	2144								16
18	9-7-66			0548	36							
	9-7-66	0542	0559	0547						19		
19	9-7-66	0718	0803	0727	31							
	9-7-66	0718	0732	0725			7	1-				
	9-7-66	0718	0803	0729						30		
	9-7-66	0720	0744	0726			08	1				
	9-7-66	0723	0803						1			
20	10-7-66	0027	0042	0035	7							
	10-7-66	0028	0058	0034						20		
21	10-7-66	0335	0347	0341	11							
	10-7-66	0336	0412	0344							1	
	10-7-66	0339	0348	0342			25	1-				
22	10-7-66	0707	0828	0723	18							
	10-7-66	0711	0815	0721			20	1-				
	10-7-66	0711	0836	0722						40		
	10-7-66	0715	0803						1			
	10-7-66	0718	0740	0720			04	1				

TABLE I CONT.

2-12 A° X-Ray Flares in July-August 1966 with Associated S.I.D.s

No.	Date	Universal Time Start	Universal Time End	Universal Time Max.	Peak 2-12 A° Flux erg x 10^{-3}/cm^2 sec	SWF Type IMP	Importance ABS	SCNA	SEA	SPA	SES	SFD
23	10-7-66	1142	1242	1155	18							
	10-7-66	1142	1300	1155						84		
	10-7-66	1145	1235	1205		S 1						
	10-7-66	1146	1157	1153			22	1				
	10-7-66	1146	1315						1			
24	10-7-66	1330	1351	1338	9							
	10-7-66	1330	1400	1340							1-	
	10-7-66	1333		1340						17		
25	10-7-66	1800	1823	1807	13							
	10-7-66	1800	1810	1802								15
	10-7-66	1800	1845	1815							2	
	10-7-66	1802	1820	1806		SL 1						
	10-7-66	1802	1900	1808						21		
26	10-7-66	1931		1951	18							
	10-7-66	1932		1945							1	
	10-7-66	1935	2015	1949			25	1				
	10-7-66	1935	2020			SL 2						
	10-7-66	1935	2220							75		
27	11-7-66	0903		0943	30							
	11-7-66	0905	1130	0945						99		
	11-7-66	0913	1010	0940			24	1				
	11-7-66	0915	1026						1			

TABLE I CONT.

2-12 A° X-Ray Flares in July-August 1966 with Associated S.I.D.s

No.	Date	Universal Time Start	End	Max.	Peak 2-12 A° Flux erg x 10^{-3}/cm^2 sec	SWF Type IMP	Importance ABS	SCNA	SEA	SPA	SES	SFD
28	12-7-66	1802	1831	1806	10							
	12-7-66	1805	1845	1815						10		
	12-7-66	1805	1845	1815							1	
	12-7-66	1808	1828	1820U		SL 1						
29	13-7-66			1251	> 50							
	13-7-66	1225	1345	1245			31	2				
30	23-7-66	0239	0323	0245	14							
	23-7-66	0239	0312	0242		S 2						
	23-7-66	0239	0327	0246								
	23-7-66	0243		0246			20	1-				
	23-7-66	0245	0339	0250							2-	
31	23-7-66	1411	1445	1418	7							
	23-7-66	1410 (?)	1440	1425		G 1-						
	23-7-66	1412	1422	1416							1-	
	23-7-66	1413	1450	1416					1			
	23-7-66	1415	1515	1422						17		
	23-7-66	1415	1515	1422								03
32	24-7-66	0031		0038	42							
	24-7-66	0039	0122	0040			30	2				
33	25-7-66	0454			> 20							
	25-7-66	0455	0540	0502						85		
	25-7-66	0456	0532	0501		S 1						
	25-7-66	0457	0538	0502			17	1-				

TABLE I CONT.

2-12 A° X-Ray Flares in July-August 1966 with Associated S.I.D.s

No.	Date	Universal Time Start	Universal Time End	Universal Time Max.	Peak 2-12 A° Flux erg X10^{-3}/cm^{2}sec	SWF Type IMP	Importance ABS	Importance SCNA	Importance SEA	Importance SPA	Importance SES	Importance SFD
34	25-7-66		1617	1545	7							
	25-7-66	1528	1620	1543						24		
	25-7-66	1532	1536	1534								07
	25-7-66	1533	1615	1547							1-	
	25-7-66	1538	1605	1545		SL 1						
35	26-7-66	0031	0116	0037	10							
	26-7-66	0032	0118	0040						36		
36	26-7-66	1157			> 10							
	26-7-66	1159	1230	1204						21		
37	26-7-66	1441	1527	1455	13							
	26-7-66	1443	1511	1450							1+	
	26-7-66	1445	1515	1455							1	
	26-7-66	1446	1530	1453						50		
	26-7-66	1450	1510	1459		SL 1+						
	26-7-66	1450	1535	1455						42		
38	28-7-66	1923		1936	3							
	28-7-66	1923	2115	1943			20	1				
39	28-7-66	2214		2328	35							
	28-7-66	2215	2217									
	28-7-66	2223	2255	2230D							2	
	28-7-66	2250	0204	2320						99		
40	2-8-66	2122	2231	2131	.9							
	2-8-66	2122	2130	2125								15
	2-8-66	2126	2139	2130			8	1				

TABLE I CONT.

2-12 A° X-Ray Flares in July-August 1966 with Associated S.I.D.s

No.	Date	Universal Time			Peak 2-12 A° Flux $erg \times 10^{-3}/cm^2 sec$	SWF Type IMP	Importance					
		Start	End	Max.			ABS	SCNA	SEA	SPA	SES	SFD
41	4-8-66		0555	0446	4							
	4-8-66	0444	0507	0450		G 1-						
	4-8-66	0444	0507	0453						12		
	4-8-66	0445	0502	0451			35	1				
42	4-8-66	2115		2124	3							
	4-8-66	2118	2158	2136		G 1+						
43	5-8-66	2314		2322	3							
	5-8-66	2316	2328	2318			17	1-				
44	6-8-66	1859	230	1908	3							
	6-8-66	1900	2030	1914					2-			
	6-8-66	1901	1907	1904								10
45	15-8-66	1109			> 8							
	15-8-66	1112	1135	1126					1-			
	15-8-66	1115	1232	1136			28	1				
46	16-8-66	2121		2124	4							
	16-8-66	2123	2131	2124						03		
47	17-8-66	0029	0103	0032	17							
	17-8-66	0030	0045	0035		G 1+						
	17-8-66	0030	0210	0033								05
	17-8-66	0031	0047	0036			15	1				
	17-8-66	0031	0115	0037						53		
48	18-8-66	1817	1855	1825	4							
	18-8-66	1818	1833	1824		SL 1-						
	18-8-66	1820	1845	1840							2	
	18-8-66	1820	1930	1840						47		

TABLE I CONT.

2-12 A° X-Ray Flares in July-August 1966 with Associated S.I.D.s

No.	Date	Universal Time			Peak 2-12 A° Flux $erg \times 10^{-3}/cm^2 sec$	SWF Type IMP	Importance					
		Start	End	Max.			ABS	SCNA	SEA	SPA	SES	SFD
49	19-8-66	0433	0510	0435	7.2							
	19-8-66	0434	0455	0441			8	1				
	19-8-66	0435	0458	0438		S 1						
	19-8-66	0437	0458	0442						18		
50	20-8-66	1842	2100	1912	4							
	20-8-66	1843	2010	1905						52		
	20-8-66	1854	1910	1856		SL 1						
51	23-8-66	1750	1831	1759	4							
	23-8-66	1754	1815			SL 1						
52	25-8-66	0618	0723	0625	15							
	25-8-66	0621	0645	0625					1-			
	25-8-66	0621	0750	0635							1	
	25-8-66	0622	0648	0628						36		
	25-8-66	0623	0636	0627			16	1-				
	25-8-66	0623	0643	0627		S 1						
53	25-8-66	1355	1442	1403	7							
	25-8-66	1357	1450	1410						38		
	25-8-66	1400	1415	1408		SL 1-						
54	26-8-66	1800	2020	1835	9							
	26-8-66	1800	1915	1835							3	
	26-8-66	1800	1950	1837						80		
	26-8-66	1810	1855	1830		G 1						
	26-8-66	1812	1816	1813								02
	26-8-66	1812	1853	1820							1+	

TABLE I CONT.

2-12 A° X-Ray Flares in July-August 1966 with Associated S.I.D.s

No.	Date	Universal Time Start	Universal Time End	Universal Time Max.	Peak 2-12 A° Flux erg x 10^{-3}/cm^{2}sec	SWF Type IMP	Importance ABS	Importance SCNA	Importance SEA	Importance SPA	Importance SES	Importance SFD
55	26-8-66		2305	2215	9							
	26-8-66	2145	2256	2230					1+			
	26-8-66	2200	0040	2217						43		
	26-8-66	2200	2255	2230							2+	
	26-8-66	2200	2300	2235			**	1				
56	27-8-66		1627	1611	4.8							
	27-8-66	1608	1700	1615						15		
	27-8-66	1610	1621	1615		G 1-						
	27-8-66	1610	1630	1618							1-	
57	27-8-66	1853	1943		> 8							
	27-8-66	1855	2000	1910						66		
	27-8-66	1900	1930	1907		SL 1						
	27-8-66	1900	2000	1915							2	
	27-8-66	1900	2030	1913					3+			
58	27-8-66	2017	2208	2056	13							
	27-8-66	2020	2125	2100		G 1+						
	27-8-66	2020	2320	2100						76		
	27-8-66	2030	2155	2040							3	
	27-8-66	2033	2258	2108					3+			
59	28-8-66	0044	0136	0053	6							
	28-8-66	0046	0128	0055		G 1-						
60	28-8-66	0509	0549	0518	7							
	28-8-66	0510	0532	0521		SL 1-						
	28-8-66	0513	0543	0530						15		

TABLE I CONT.

2-12 A° X-Ray Flares in July-August 1966 with Associated S.I.D.s

No.	Date	Universal Time Start	Universal Time End	Universal Time Max.	Peak 2-12 A° Flux ergX10^{-3}/cm^{2}sec	SWF Type IMP	Importance ABS	Importance SCNA	Importance SEA	Importance SPA	Importance SES	Importance SFD
61	28-8-66	1522		1531	188							
	28-8-66	1523	1600	1527								235
	28-8-66	1523	1615	1530					3			
	28-8-66	1523	1730	1533						99		
	28-8-66	1524	1700	1530		S 3+						
	28-8-66	1525	1526									
	28-8-66	1526	1620						1			
	28-8-66	1526	1715	1535					3			
	28-8-66	1526	1720	1530							2+	
	28-8-66	1527	1547	1530								
	28-8-66	1527	1619	1532			95	3				
62	28-8-66	2131	2142	2135	6.4							
	28-8-66	2131	2135	2133								15
	28-8-66	2132	2337	2135						34		
63	29-8-66		0616	0546	10							
	29-8-66	0536	0552	0546			12	1-				
	29-8-66	0538	0600	0546		G 1-						
	29-8-66	0539	0610	0551						20		
64	30-8-66	1447		1514	34							
	30-8-66	1450	1630	1505						99		
	30-8-66	1451	1459	1454								17
	30-8-66	1455	1535						1			
	30-8-66	1455	1545	1515							2	
	30-8-66	1455	1552	1503			41	2				
	30-8-66	1455	1554	1517		SL 2+						
	30-8-66	1455	1600	1505					3			

TABLE I CONT.

2-12 A° X-Ray Flares in July-August 1966 with Associated S.I.D.s

No.	Date	Universal Time Start	Universal Time End	Universal Time Max.	Peak 2-12 A° Flux $erg x 10^{-3}/cm^2 sec$	SWF Type IMP.	Importance ABS	Importance SCNA	Importance SEA	Importance SPA	Importance SES	Importance SFD
	30-8-66	1457	1520	1501			16	1				
	30-8-66	1511	1518	1512								15
65	31-8-66	0036		0106	45							
	31-8-66	0038	0450	0106						99		
	31-8-66	0040	0440	0258		G 3						
	31-8-66	0040	0449	0051			30	2				
66	31-8-66	1829		1840	5.5							
	31-8-66	1831	1835	1832								05
	31-8-66	1836	1920	1906		G 2						
	31-8-66	1848		1900						42		
	31-8-66	1850	1856	1851								06
67	31-8-66	1900			> 10							
	31-8-66	1904	1909	1905								02
	31-8-66	1905	1935	1912							1+	

TABLE II

Variation of ρ(h) and N(h) with Height

Height km	log ρ(h) cm^{-3}	log N(h) cm^{-2}
60	15.80	21.67
65	15.55	21.37
70	15.26	21.04
75	14.95	20.70
80	14.60	20.35
85	14.19	19.95
90	13.80	19.55
95	13.40	19.16
100	13.00	18.80

REFERENCES

Belrose, J. S., and M. J. Burke, J. Geophys. Res. 69, 2799 (1964).

Biondi, M. A., Ann. Geophys. 20, 5 (1964).

CIRA - 1965, Compiled by working group IV of the Committee on Space Research, (North Holland Publishing Co., 1965).

Deeks, D. G., Private Communication, 1964.

Doering, J. P., and B. H. Mahan, J. Chem. Phys. 36, 669 (1962).

Friedman, H., Ann. Geophys. 17, 245 (1961).

Mitra, A. P., The Penn. State University Sci. Rept. 145 (1961).

Mitra, A. P., Private Communication, R. P. U., N. P. L., India (1964).

Nicolet, M., Electron Density Profiles, (New York: The Macmillan Co., 1962), pp. 116.

Neupert, W. M., The Physics of Solar Flare, NASA 49 (1963).

Sengupta, P. R., "X-Ray Emission from the Quiescent Sun," Private communication (U. of Iowa Res. Rept. 68-12) (1968).

Sengupta, P. R., "Solar X-Ray Flares," Private Communication (U. of Iowa Res. Rept. 68-11) (1968).

Smith, L. G., Private Communication, (1963).

Van Allen, J. A., U. of Iowa Res. Rept. No. 67-35 (1967).

Webber, W. R., J. Geophys. Res. 67, 5091 (1962).

Whitten, R. C., and I. G. Poppof, Physics of the Lower Ionosphere, (Prentice-Hall, 1965), pp. 16.

FIGURE CAPTIONS

FIGURE 1. Arrangement of detectors on Explorer 33.

FIGURE 2. $F(\alpha)$ plot for GMI.

FIGURE 3. GMI sectoring scheme.

FIGURE 4. Absolute photon efficiency of U.I. x-ray detector on Explorer 33.

FIGURE 5. Absolute energy flux efficiency of U.I. detector on Explorer 33.

FIGURE 6. σ for Molecular oxygen.

FIGURE 7. σ for Molecular nitrogen.

FIGURE 8. Computed heights of unit optical depth for different λ.

FIGURE 9. Computed electron production rate per unit flux for $\lambda = 2$ A°, 5 A° and 8 A°, $\chi = 0$.

FIGURE 10. Quiescent sun x-ray spectral energy distribution.

FIGURE 11. Computed electron production rates due to quiescent sun x-rays, Lyman alpha and galactic cosmic radiation and also observed electron production rate.

G68-115-1

ARRANGEMENT OF DETECTORS ON EXPLORER-33

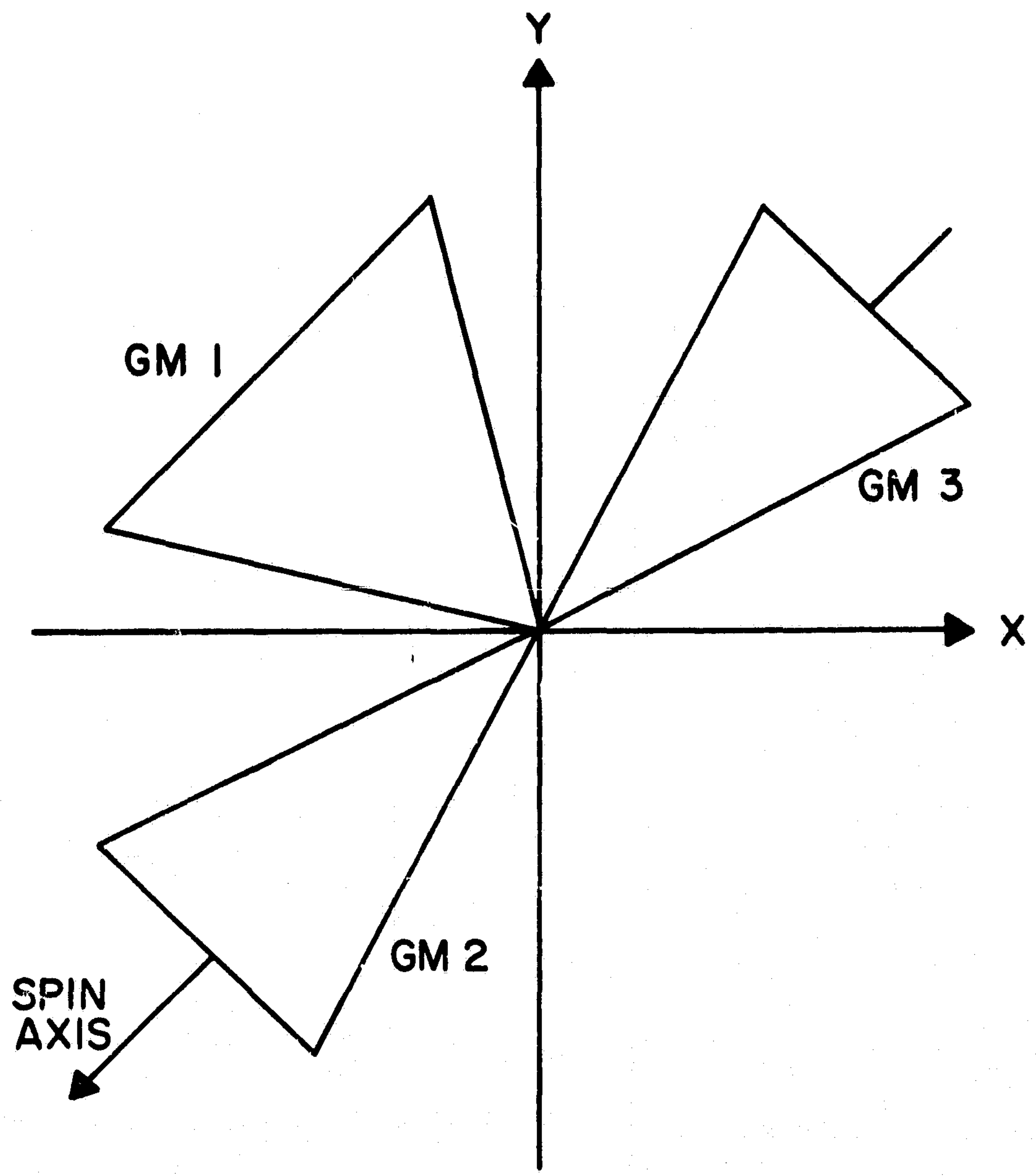

FIG-1

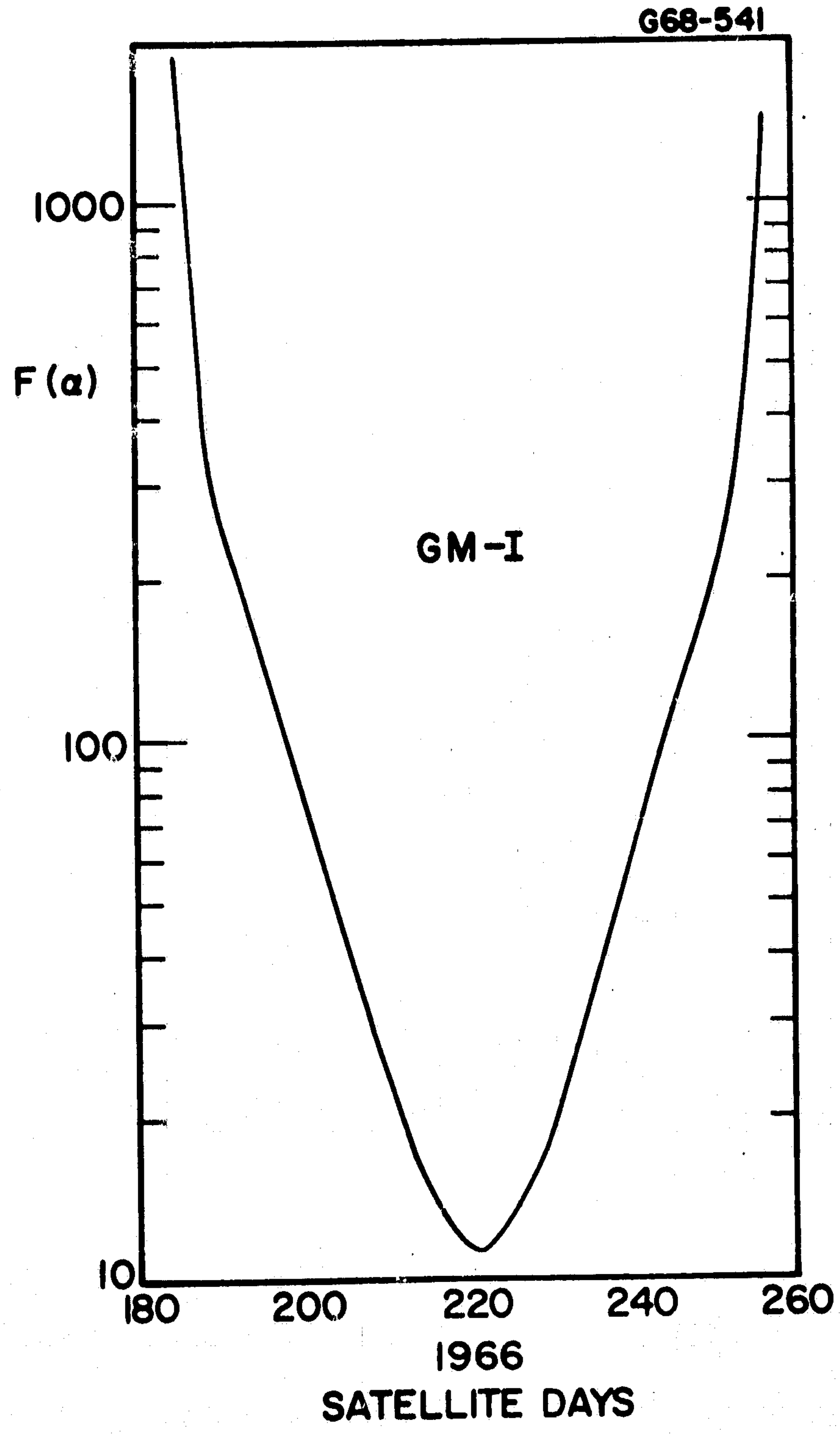
G68-541
1000
100
10
F (a)
GM-I
180
200
220
240
260
1966
SATELLITE DAYS

FIG.2

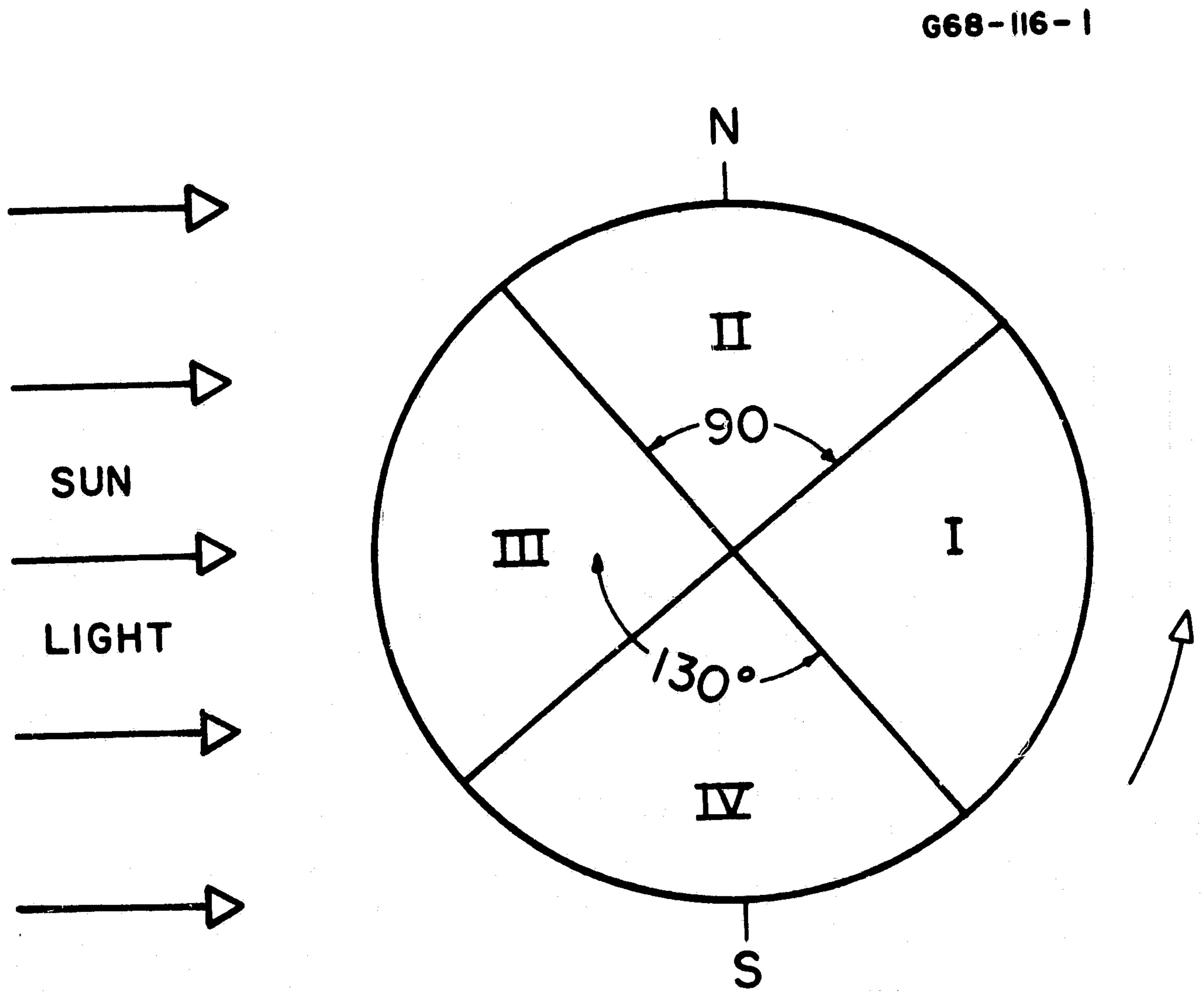

GMI SECTORING SCHEME—[EXPLORER-33]

FIG.-3

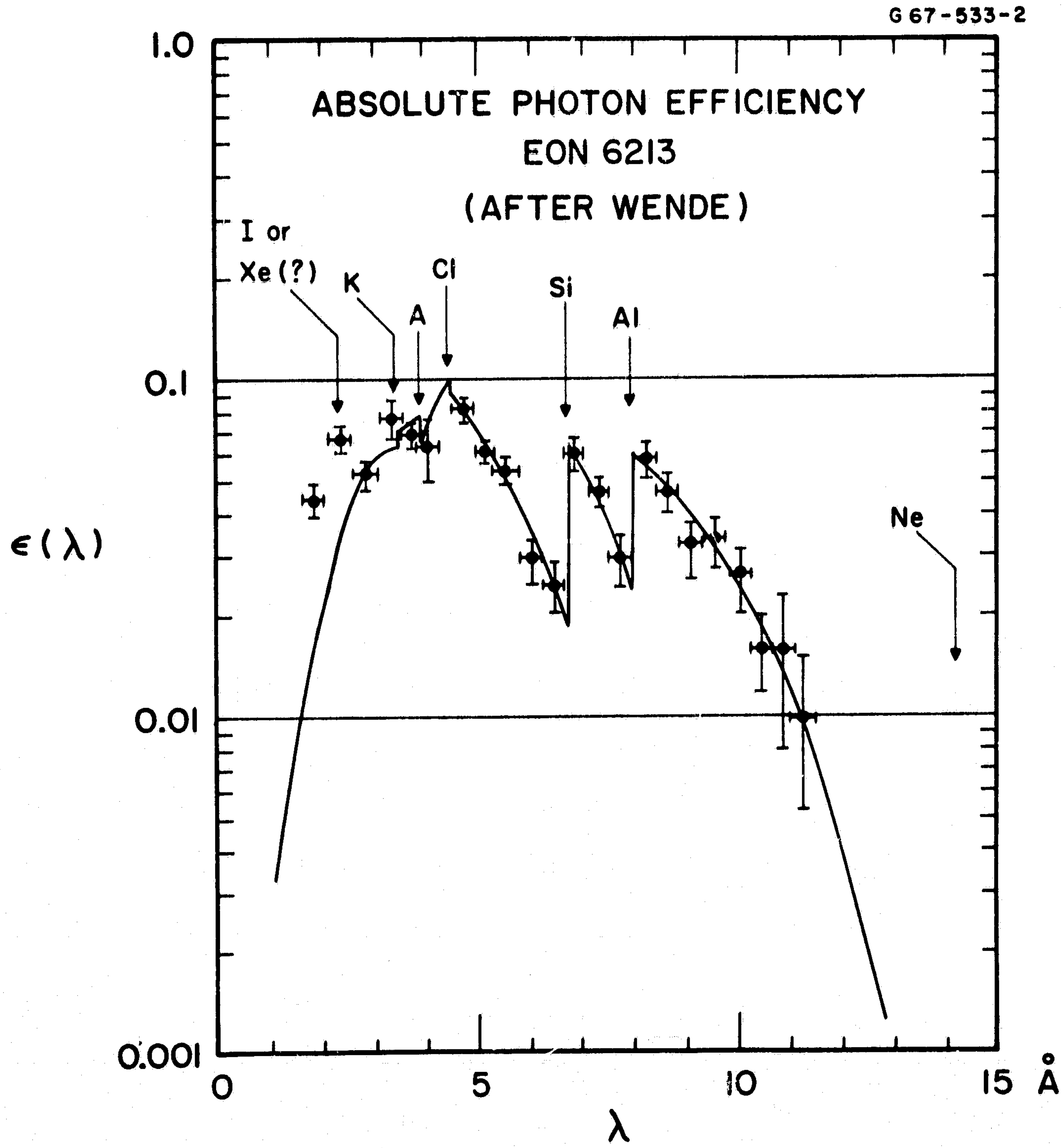
G 67-533-2
ABSOLUTE PHOTON EFFICIENCY
EON 6213
(AFTER WENDE)
I or
Xe (?)
K
A
Cl
Si
Al
Ne
1.0
0.1
0.01
0.001
ε(λ)
0
5
10
15 Å
λ

FIG. 4

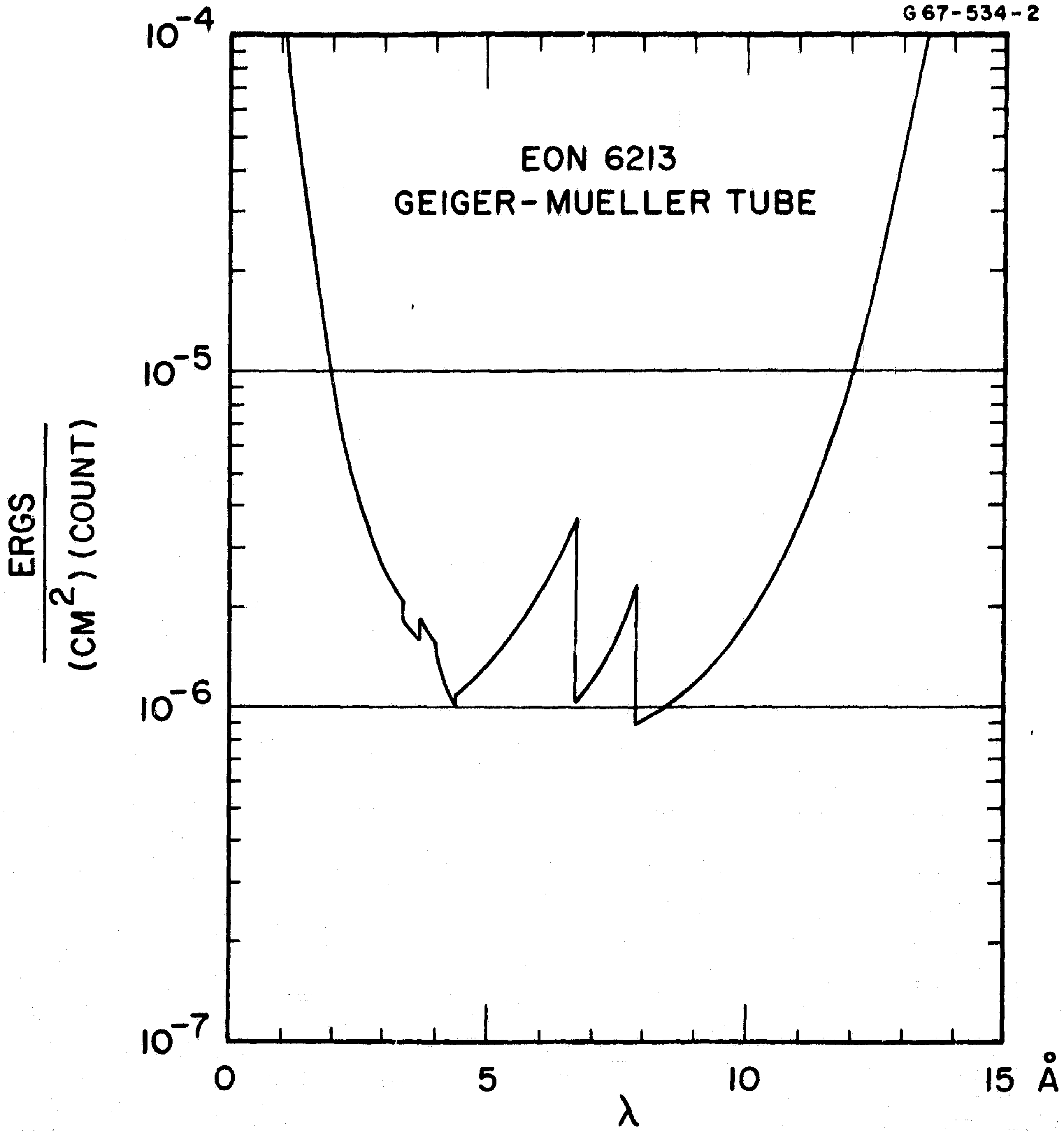

FIG. 5
ABSOLUTE ENERGY FLUX EFFICIENCY OF GM-I

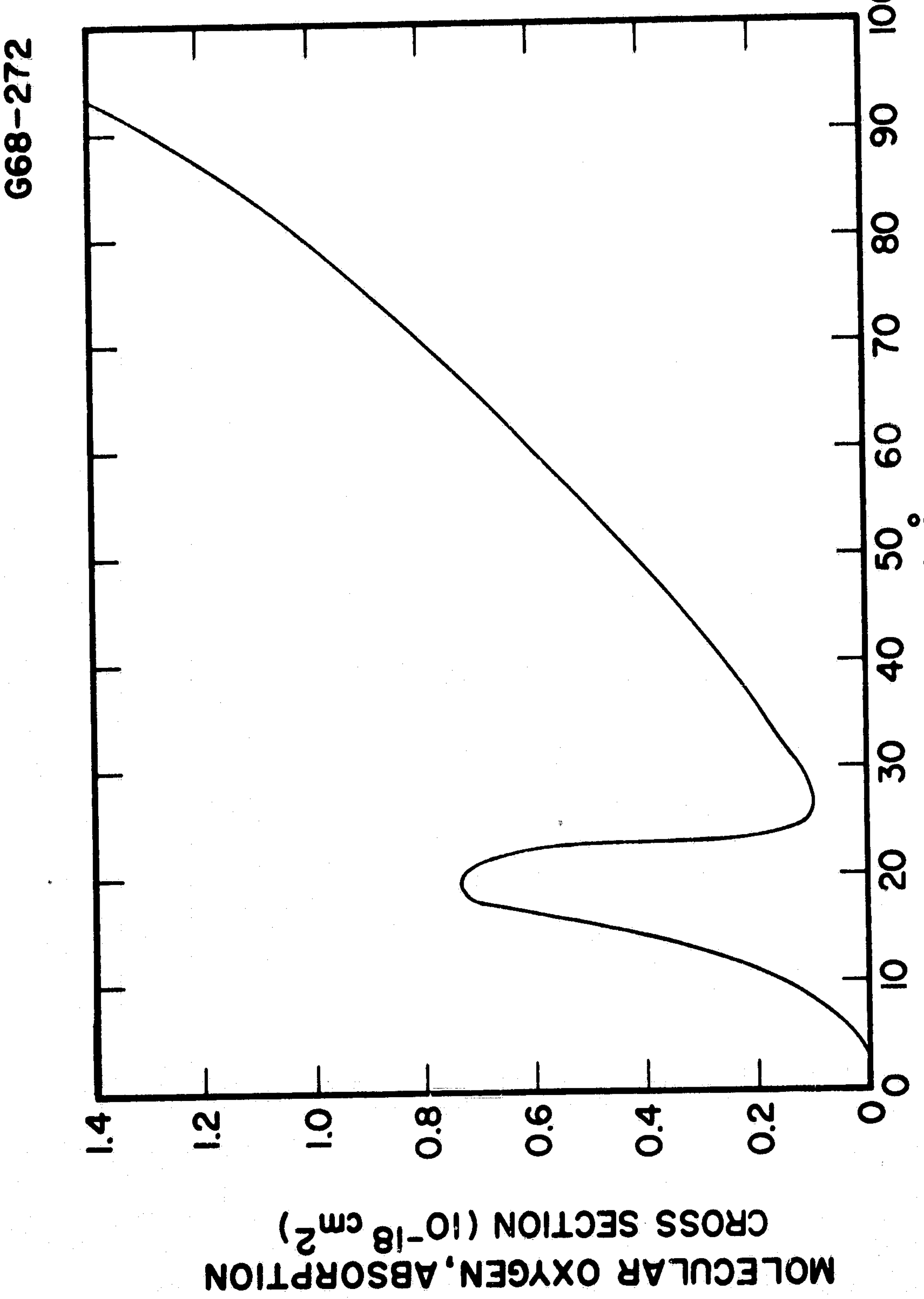

FIG. 6 ABSORPTION CROSS SECTIONS FOR MOLECULAR OXYGEN.

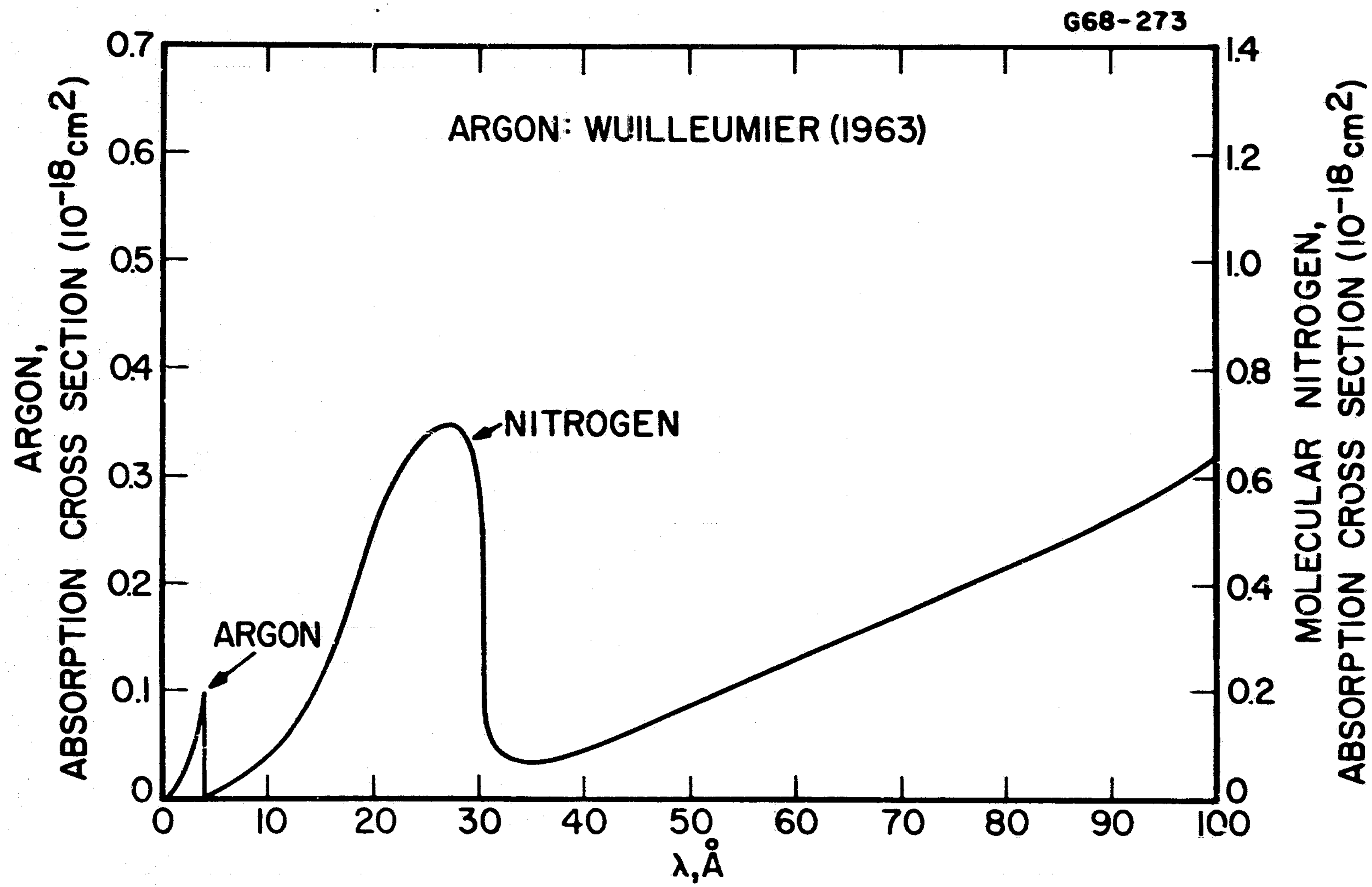

FIG. 7. ABSORPTION CROSS SECTIONS FOR MOLECULAR NITROGEN AND FOR ARGON.

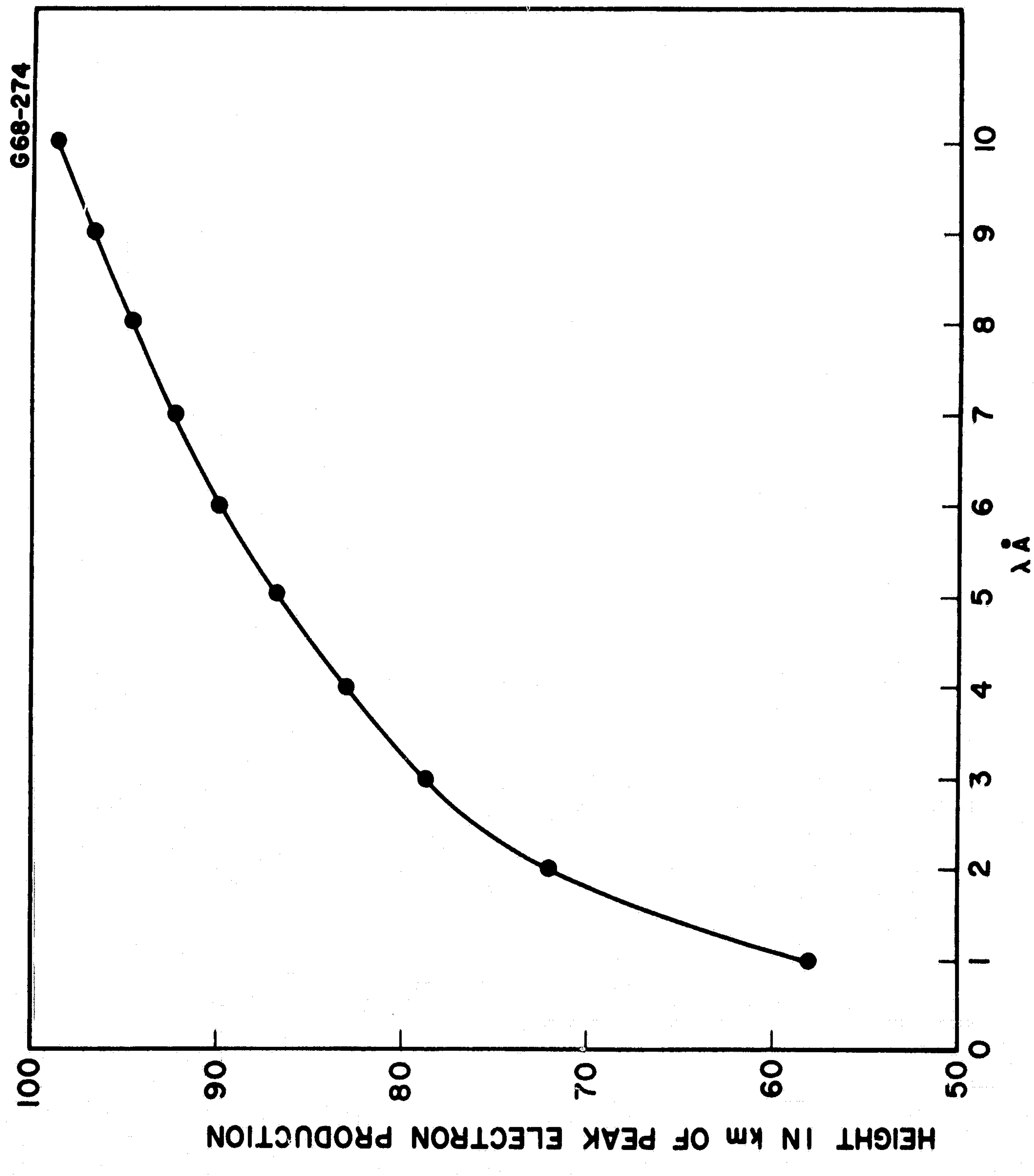
G68-274
HEIGHT IN km OF PEAK ELECTRON PRODUCTION
100
90
80
70
60
50
0
1
2
3
4
5
6
7
8
9
10
λ Å

FIG.8

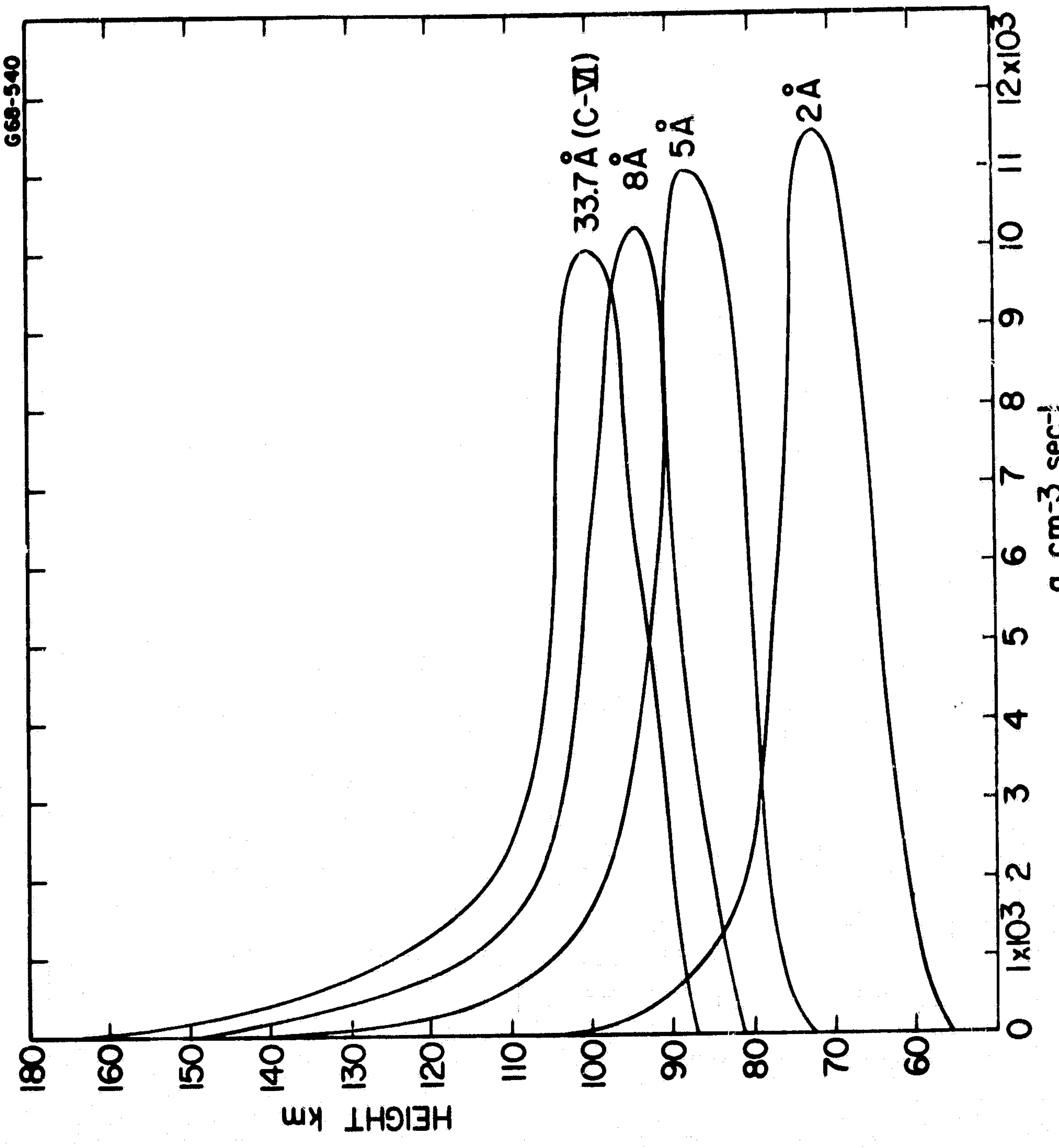
G68-540
33.7 Å (C-VI)
8 Å
5 Å
2 Å
HEIGHT km
180
160
150
140
130
120
110
100
90
80
70
60
0
1x103
2
3
4
5
6
7
8
9
10
11
12x103
q cm-3 sec-1

FIG.9

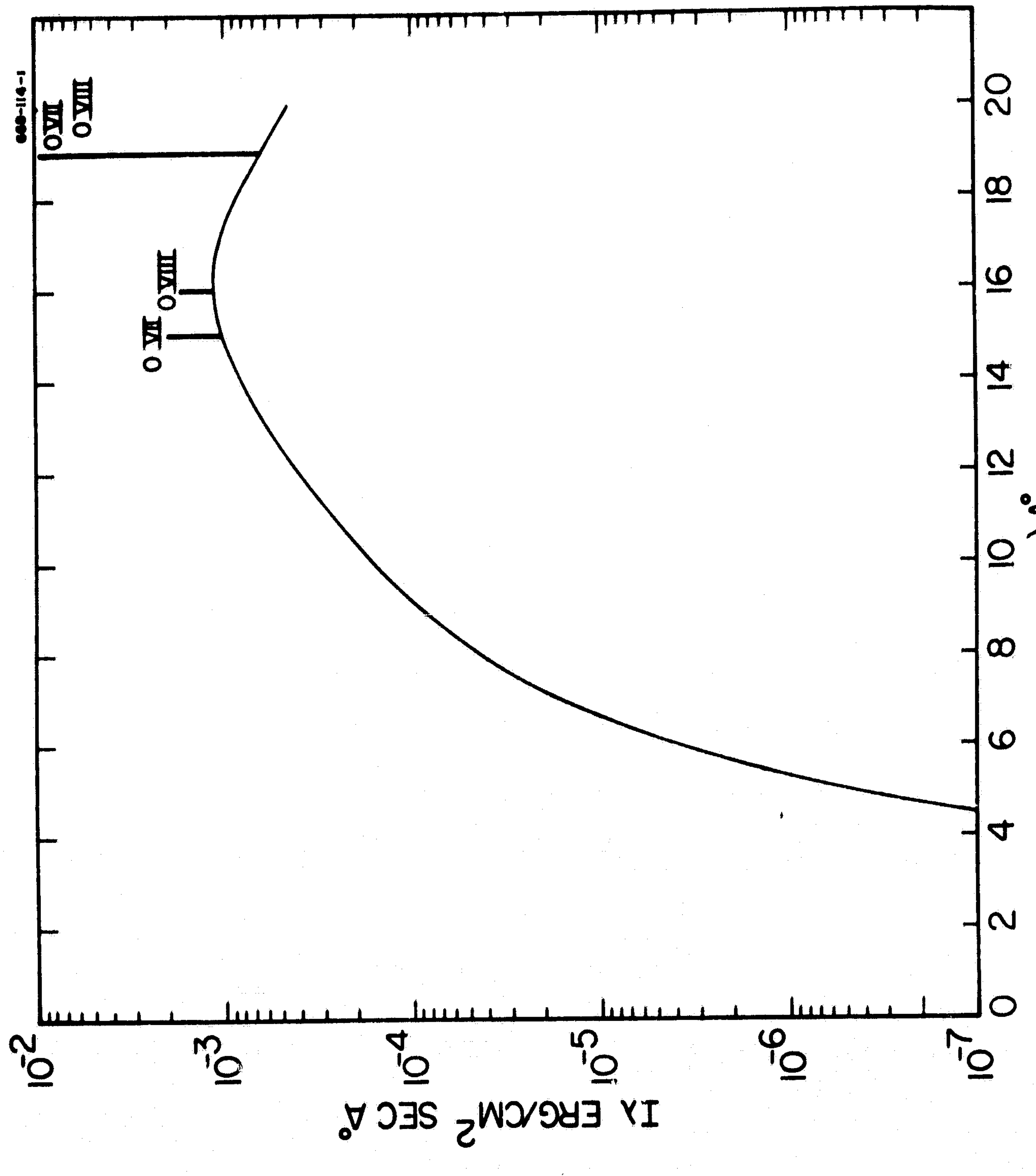
Iλ ERG/CM² SEC A°
10⁻²
10⁻³
10⁻⁴
10⁻⁵
10⁻⁶
10⁻⁷
0
2
4
6
8
10
12
14
16
18
20
λA°
O VII
O VIII
O VII
O VIII

FIG 10

G68-554

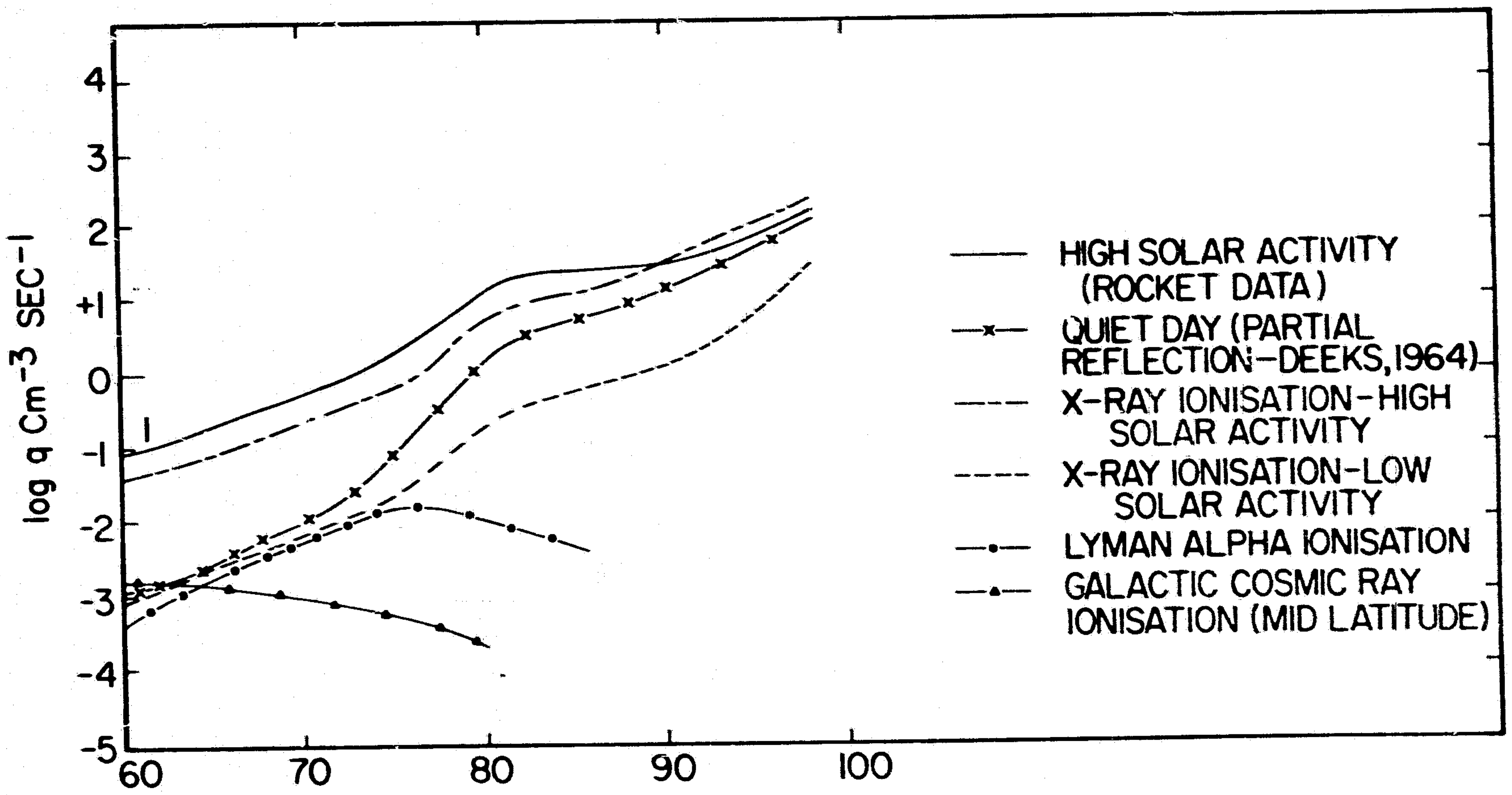

FIG. II

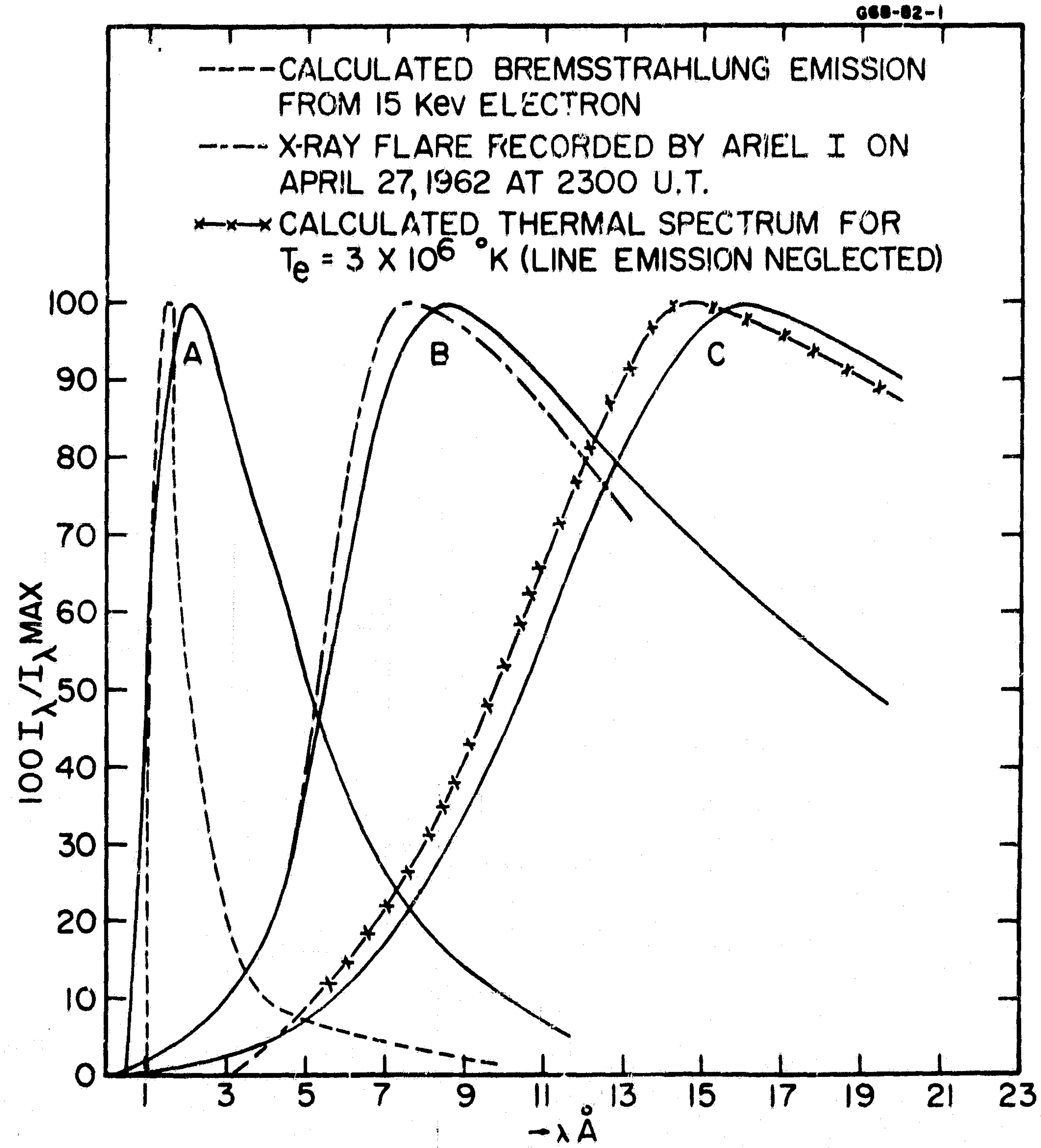
G68-82-1
----CALCULATED BREMSSTRAHLUNG EMISSION FROM 15 Kev ELECTRON
-·-·- X-RAY FLARE RECORDED BY ARIEL I ON APRIL 27, 1962 AT 2300 U.T.
×—×—× CALCULATED THERMAL SPECTRUM FOR $T_e = 3 \times 10^6$ °K (LINE EMISSION NEGLECTED)
$100 I_\lambda / I_\lambda MAX$
0
10
20
30
40
50
60
70
80
90
100
A
B
C
1
3
5
7
9
11
13
15
17
19
21
23
→λ Å

FIG 12

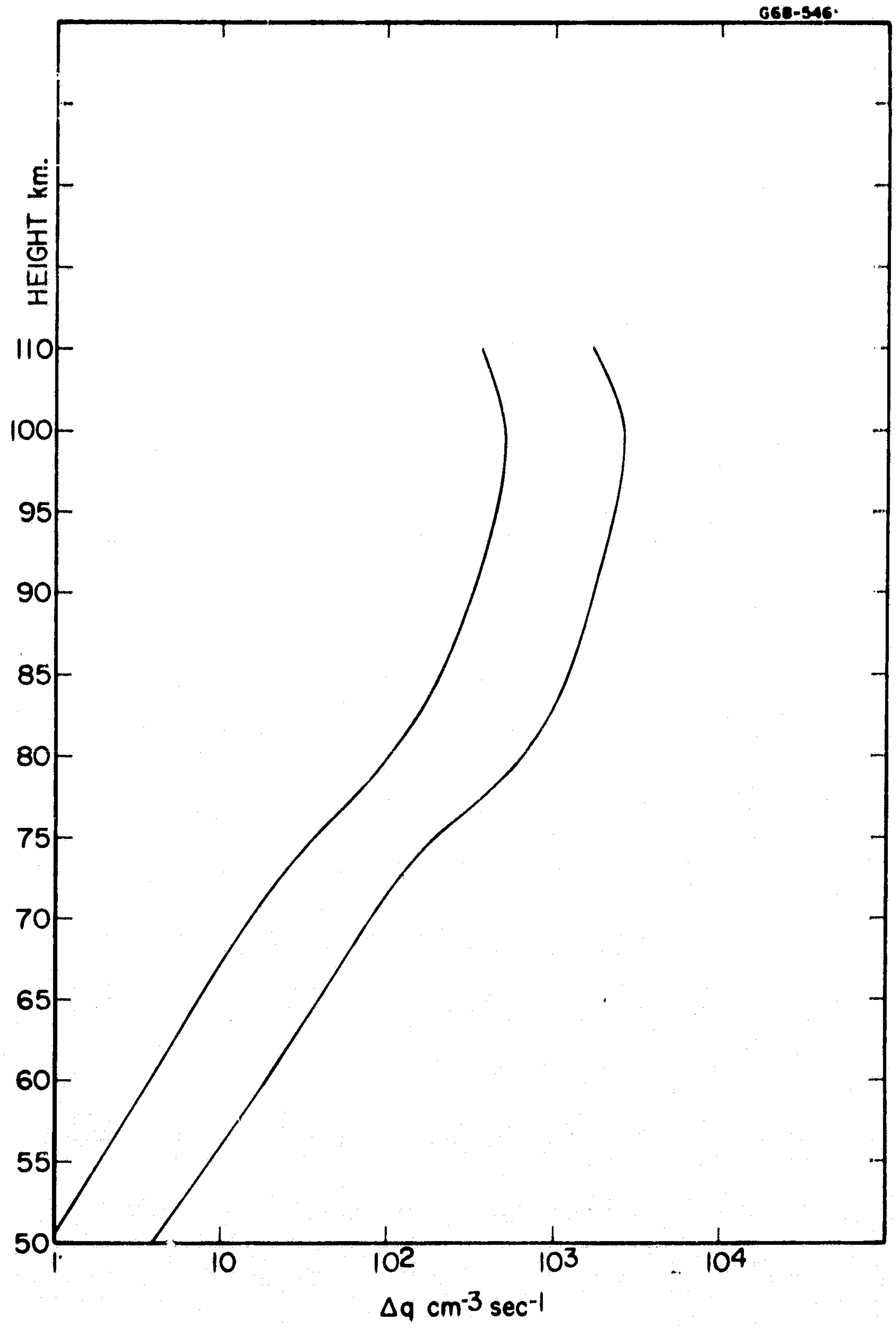
G68-546
HEIGHT km.
110
100
95
90
85
80
75
70
65
60
55
50
1
10
10^2
10^3
10^4
Δq cm^{-3} sec^{-1}

FIG. 13

G68-278

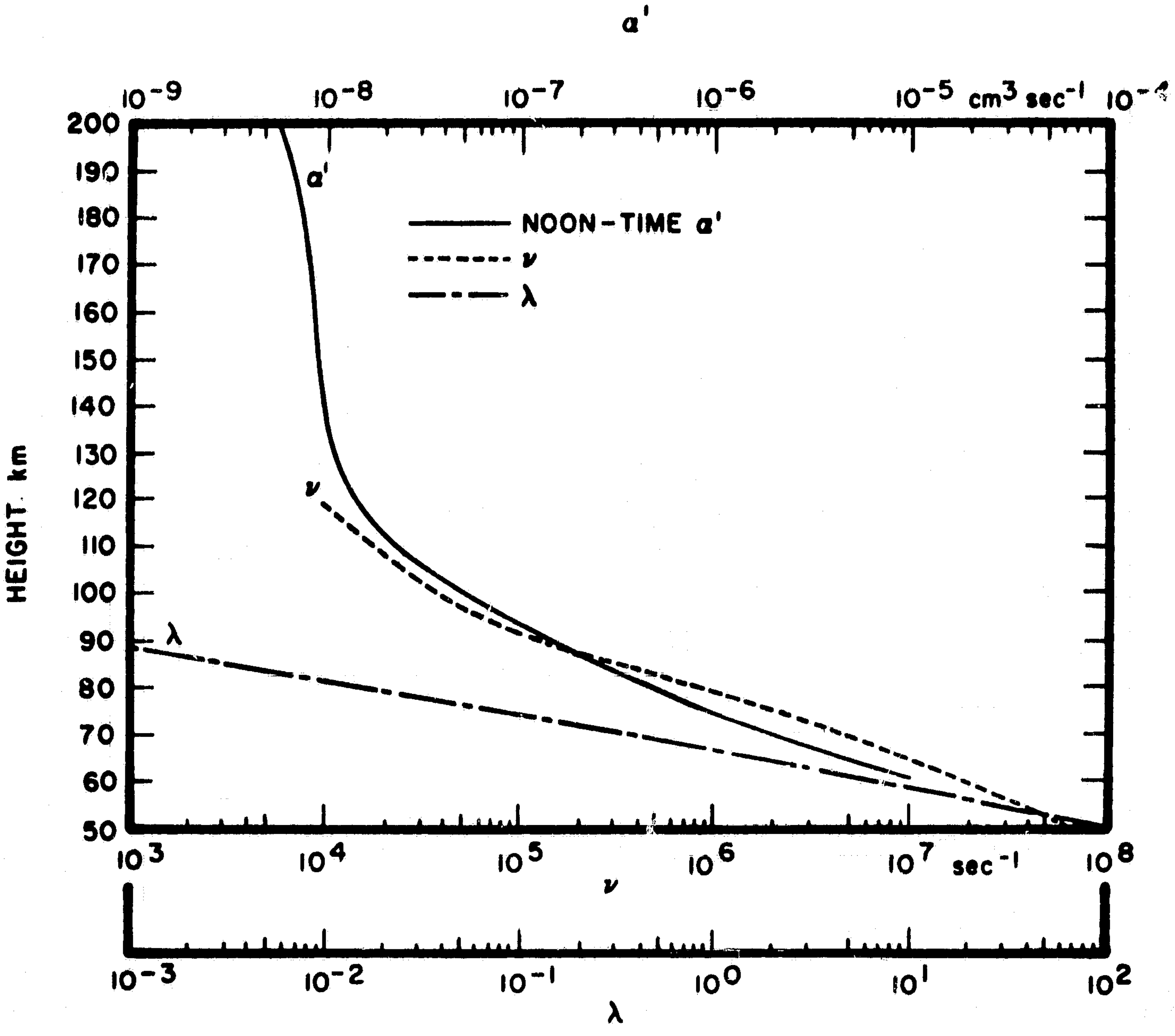

(b) DAYTIME MODELS OF THE EFFECTIVE RECOMBINATION COEFFICIENT (a'), COLLISION FREQUENCY (ν), AND THE RATIO OF NEGATIVE IONS TO ELECTRONS (λ_n)

FIG. 14 MODELS OF IONOSPHERIC PARAMETERS

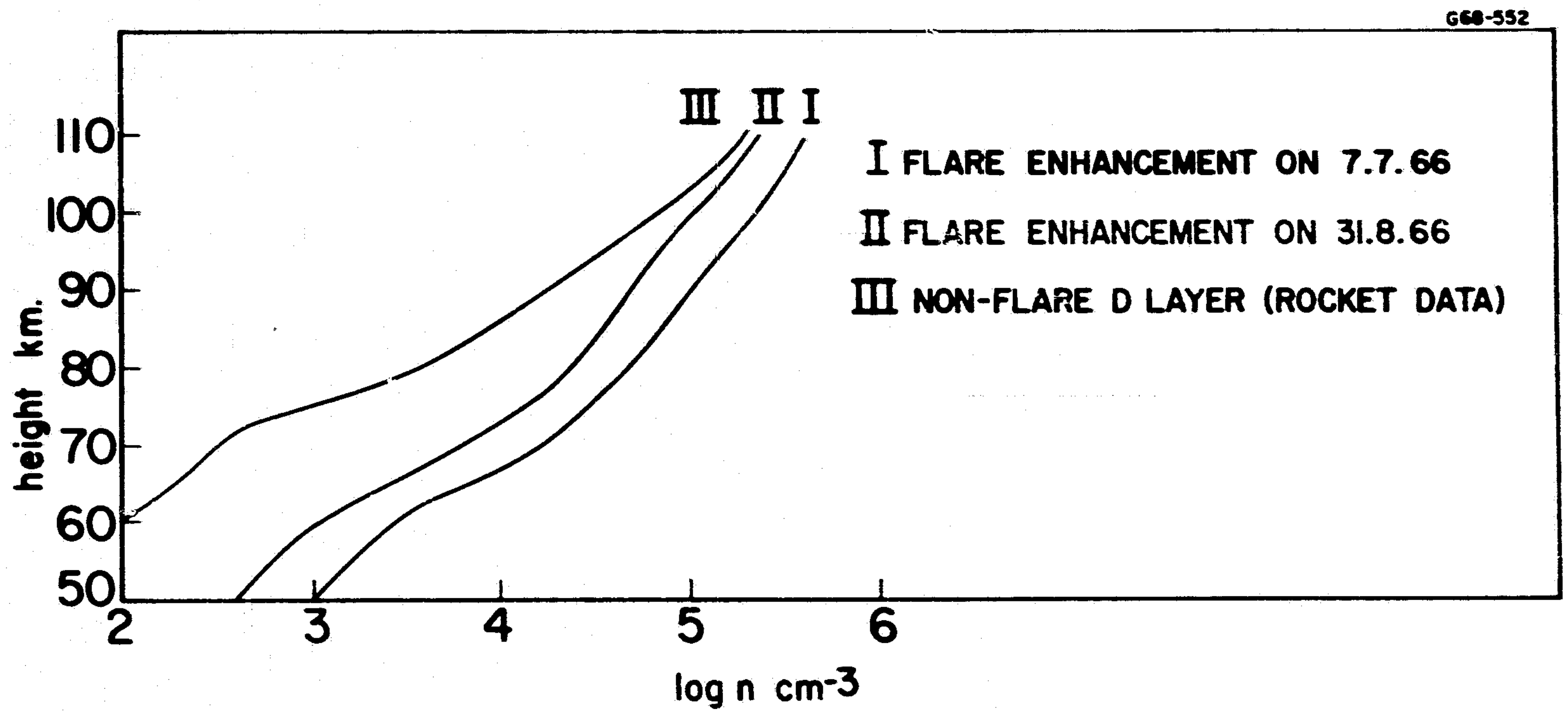
G68-552
III II I
I FLARE ENHANCEMENT ON 7.7.66
II FLARE ENHANCEMENT ON 31.8.66
III NON-FLARE D LAYER (ROCKET DATA)
height km.
110
100
90
80
70
60
50
2
3
4
5
6
log n cm-3

FIG. 15

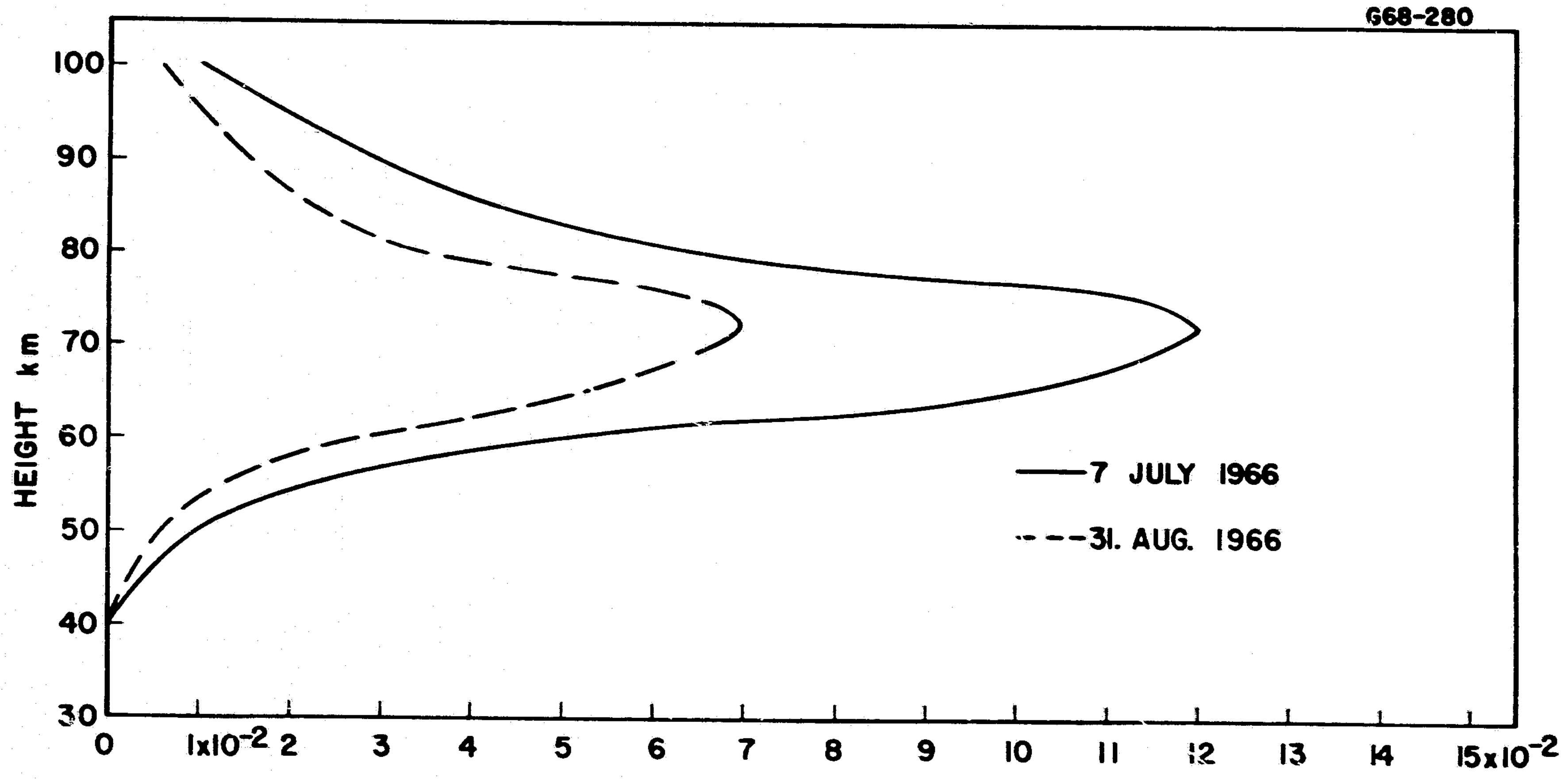
G68-280
HEIGHT km
100
90
80
70
60
50
40
30
0
1x10-2
2
3
4
5
6
7
8
9
10
11
12
13
14
15x10-2
—7 JULY 1966
---31. AUG. 1966
—ABSORPTION db/km

FIG. 16

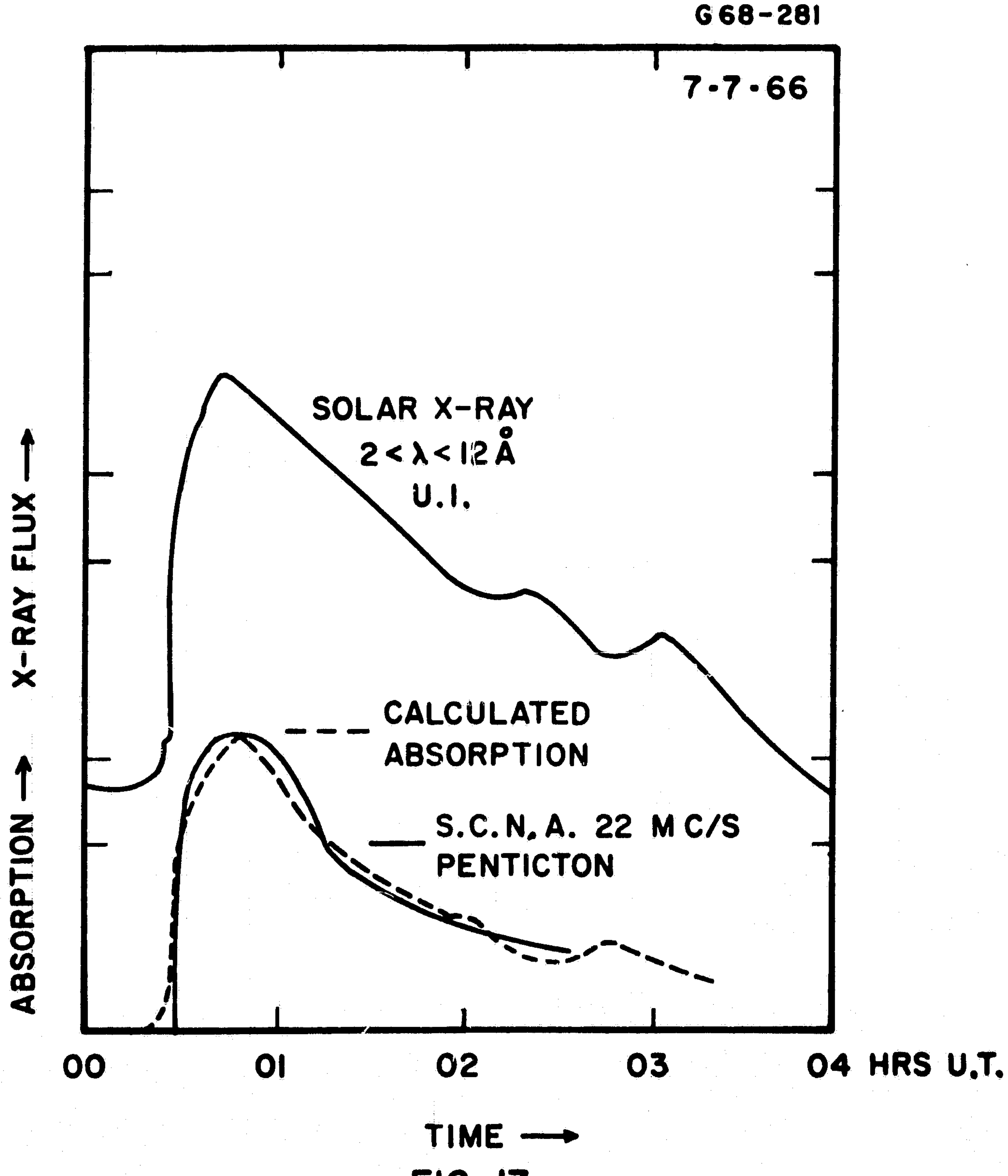
G68-281
7·7·66
SOLAR X-RAY
2 < λ < 12 Å
U.I.
CALCULATED
ABSORPTION
S.C.N.A. 22 MC/S
PENTICTON
ABSORPTION → X-RAY FLUX →
00
01
02
03
04 HRS U.T.
TIME →

FIG. 17

U. of Iowa 68-17

ERRATA

"Effect of $\lambda < 10$ A° Solar X-Rays on the Ionosphere between 60 and 100 km," by P. R. SENGUPTA

Page 5, line 10

Change "Starker" to "Straker"

Page 16, line 17

Change "decreases" to "decrease"

Page 18, line 14

Change [Neupert, 1964] to [Whitten and Popoff, 1965]